# A Seysen's Algorithm based Incremental Lattice Reduction

Qinwei He, Yulin Hu, Anke Schmeink

**Abstract**

Lattice reduction (LR) aided detections have attracted great attention in the symbol detection of multiple-input multiple-out (MIMO) communication, especially for systems with larger scale antennas. Recently, the Lenstra-Lenstra-Lovász (LLL) based incremental LR (ILR) algorithms have been proposed to employ an early termination to jointly conduct the LR and retrieve the symbol based on a partial successive interference cancellation (SIC) detection, which induces a significant performance improvement. In this paper, we propose to apply the Seysen's algorithm (SA) to the ILR. After providing the feasibility analysis, two novel SA involved algorithms are introduced and studied. Particularly, a new sorted QR decomposition based SA algorithm is proposed and tested as it plays a key role in the SIC detection. Subsequently, a novel SA based ILR scheme is further developed and investigated. By simulations, we show that the proposed approach outperforms conventional LLL based ILR in various aspects, while only a marginal increment in the complexity, restricted to medium SNR regions, is observed.

## I. Introduction

In order to meet the demands on the high transmission capacity and spectral efficiency requirements of modern wireless communication systems [1], the multiple-input multiple-out (MIMO) technique has been proposed and is regarded as an appropriate solution, owing its capability to provide multiplexing and diversity gain without requiring additional spectral resources. More recently, evolving from the conventional MIMO technique, massive MIMO, which employs very large number of antennas, has attracted great attention and will play a crucial role in 5G [2], [3]. To take the full advantage of it, an efficient symbol detection must be conducted at the receiver side. It is well-known that the maximum likelihood (ML) detector could provide the optimal symbol detection and the sphere decoder is usually employed to approximate this optimal solution [4], while the high complexity prohibits them from a practical implementation for MIMO systems, especially the one with a large number of antennas and high modulation orders. Hence, suboptimal linear and nonlinear detectors with low complexity are often employed [5], [6], [7]. However, these schemes cannot obtain the full receive diversity and experience a significant performance loss. Observing this, the lattice reduction (LR) technique is introduced to improve their performance [8], [9], [10], [11]. It has been proven that the LR-aided linear [12] and successive interference cancellation (SIC) [13] detectors are able to achieve the same diversity order as the ML detector, as the LR provides a near orthogonal channel matrix to reform the system model [14].

Moreover, a lot of research has been done to directly reduce the complexity of LR algorithms. In particular, as enjoying a polynomial computational complexity, the Lenstra-Lenstra-Lovász (LLL) algorithm has been wildly considered in the LR-aided MIMO detection [15], [16]. An effective LLL algorithm is proposed in [17], it reduces the complexity of the original one by only conducting the size reduction on pairs of the consecutive basis vectors. In [18], a complex value based LLL (CLLL) is introduced with an ability to reduce the size of the channel matrix by half. In order to bound the complexity of the LLL, a fixed-complexity LLL (fcLLL) is proposed in [19]. The methods to further reduce the complexity of fcLLL can be found in [20], [21], [22]. Instead of only treating the LR and detection as two separate parts, an approach referred to as incremental LR (ILR) is recently proposed in [23], which optimises the LR and SIC process simultaneously. It is realized by utilizing a reliability assessment (RA) [24], [25] to early terminate (ET) the intermediate process of LR.

However, all the above studies are based on LLL, which has the following limitations: i.) The orthogonality of the LLL-reduced basis can still be further improved; ii.) The LLL can only find an orthogonal

basis of the lattice which is spanned by the channel matrix. The inverse of the channel matrix is not taken into consideration in the LR process. Therefore, this motivates us to study an alternative and promising LR scheme, the Seysen's Algorithm (SA) [26]. Some SA variants with reduced complexity are also proposed in [27], [28]. And the SA based detectors are introduced and evaluated in [29], [30]. However, the SA has not been extended to the ILR yet.

In this paper, we propose to apply the SA instead of the LLL algorithms in the ILR operation. After providing the feasibility analysis, we first introduce a novel sorted QR decomposition (SQR) based SA, which is realized by updating the output matrices $\mathbf{Q}$ and $\mathbf{R}$ from the SQR iteratively. It enables us to conduct an SIC detection directly in the intermediate step of the SA reduction, which is crucial as the conventional SA algorithms cannot provide the necessary $\mathbf{Q}$ and $\mathbf{R}$ immediately to facilitate this SIC detection and the ILR must perform the ET based on this detection. With the help of the SQR based SA, a novel SA based ILR algorithm is introduced and studied.

The remainder of this paper is organized as follows. In Section II, the system model, LR-aided detection techniques and LR methods are introduced. We validate the feasibility of employing SA to the ILR scheme at the beginning of Section III. And two proposed SA related algorithms are elaborated in this section as well. The performance of these algorithms are evaluated based on the simulation results in Section IV. Finally, Section V concludes this paper.

*Notation:* The super scripts $(\cdot)^T$, $(\cdot)^*$ and $(\cdot)^{\mathcal{H}}$ denote the transpose, conjugate and Hermitian, respectively. The matrices and column vectors are represented by upper and lower bold face letters. We denote the $n$-th element of a vector $\mathbf{h}$ by $h_n$ and the $(m,n)$-th entry of matrix $\mathbf{H}$ by $H_{m,n}$. A submatrix of $\mathbf{H}$ with elements of the $a$-th to the $b$-th row and the $c$-th to the $d$-th column is represented by the bold italic letter $\boldsymbol{H}_{a:b,c:d}$. If all the rows or columns are selected, the subscript can be shortened to $:$ . Thus the $i$-th column vector of $\mathbf{H}$ is $\boldsymbol{H}_{:,i}$. We reserve $E[\cdot]$ for the expectation, $|\cdot|$ for the absolute value of a scalar, $\|\cdot\|$ for the 2-norm of a vector, $\Re(\cdot)$ and $\Im(\cdot)$ for the real and imaginary parts.

## II. Preliminaries

In this section, we first introduce the system model and the associated LR aided detections. Subsequently, an overview of LLL and SA is given.

### A. System Model

In this section, we first introduce the system model and then describe the associated traditional detection methods. A MIMO system with $N_t$ transmit and $N_r$ receive antennas is considered here, and in particular, we assume $N_t \leq N_r$. Denote by $\mathbf{s}$ the transmitted symbol. Thus, $\mathbf{s}$ is an $N_t \times 1$ vector $[s_1, s_2, \ldots, s_{N_t}]^T$, while each entry of the vector is an element of a constellation set $\mathcal{M}$, i.e., $s_i \in \mathcal{M}$, where $i = 1, 2 \ldots, N_t$. Moreover, we assume that the transmitting power of each antenna is one, which means $E\left[\mathbf{s}\mathbf{s}^{\mathcal{H}}\right] = \mathbf{I}_{N_t}$. Matrix $\mathbf{H}$ denotes the channel matrix of size $N_r \times N_t$, which remains unchanged at each signalling interval. Note that $\mathbf{H}$ represents a general channel matrix, i.e., could represent either canonical or spatial correlation channels. We assume the system is perfectly synchronised and the channel state information (CSI) is known at the receiver. Thus, the received $N_r \times 1$ vector $\mathbf{y}$ is

$$\mathbf{y} = \mathbf{H}\mathbf{s} + \mathbf{n}, \tag{1}$$

where $\mathbf{n}$ is the additive white Gaussian noise (AWGN) vector with zero mean and covariance matrix $E\left[\mathbf{n}\mathbf{n}^{\mathcal{H}}\right] = \sigma_n^2 \mathbf{I}_{N_r}$. Therefore, the signal-to-noise ratio (SNR) of each antenna at the receiver side is given as $\mathrm{SNR} = \frac{N_t E\left[\mathbf{s}^{\mathcal{H}}\mathbf{s}\right]}{\sigma_n^2}$.

Obviously, in order to retrieve the transmitted symbol $\mathbf{s}$ at the receiver side, a detector is necessary. The optimal solution is the maximum likelihood (ML) detector. However, the complexity of it grows exponentially with the size of the constellation set $\mathcal{M}$ and the number of transmit antennas $N_t$, which makes it infeasible for practical systems. To reduce the complexity, the detections with suboptimal solutions are used more commonly, including the linear and nonlinear cases.

Generally, there are two types of linear detections, i.e., ZF and MMSE. The ZF detector only requires knowledge of the channel matrix $\mathbf{H}$ while the MMSE detector also takes the power of the Gaussian noise $\sigma_n^2$ into consideration. With the introduction of the extended system [31], the equalised signal of both ZF and MMSE detector can be represented as

$$\mathbf{s}^{\mathrm{eq}} = \mathbf{H}^{\dagger}\mathbf{y}, \tag{2}$$

where $\mathbf{H}^{\dagger} = \left(\mathbf{H}^{\mathcal{H}}\mathbf{H}\right)^{-1}\mathbf{H}^{\mathcal{H}}$ denotes the Moore-Penrose pseudo-inverse of the channel matrix (or the augmented channel matrix for the MMSE detector). After equalisation, each element of $\mathbf{s}^{\mathrm{eq}}$ has to be quantised to the nearest constellation point to finish this detection, i.e., $\hat{\mathbf{s}} = \mathcal{Q}_{\mathcal{M}}\left(\mathbf{s}^{\mathrm{eq}}\right)$, where $\mathcal{Q}_{\mathcal{M}}$ is the quantisation function.

On the other hand, nonlinear SIC detection is also frequently used in practice. In the SIC, a QR decomposition is applied to the channel matrix, i.e., $\mathbf{H} = \mathbf{QR}$, where $\mathbf{Q}$ is an $N_r \times N_t$ orthogonal matrix with orthonormal columns and $\mathbf{R}$ is an upper triangular matrix. Particularly, there exists a unique QR factorisation if the diagonal elements of $\mathbf{R}$ are required to be positive. Throughout this paper, we assume this condition is fulfilled. Obviously, if we left multiply matrix $\mathbf{R}$ to both sides of Equation (2), the expression is simplified to

$$\mathbf{R}\mathbf{s}^{\mathrm{eq}} = \mathbf{v}, \tag{3}$$

where $\mathbf{v} = \mathbf{Q}^{\mathcal{H}}\mathbf{y}$. As $\mathbf{R}$ is an upper triangular matrix, one can get the equalised last entry of vector $\mathbf{s}^{\mathrm{eq}}$ by a simple division, which is $s_{N_t}^{\mathrm{SIC}} = v_{N_t}/R_{N_t,N_t}$. Then, the estimated value of it can be calculated by $\hat{s}_{N_t}^{\mathrm{SIC}} = \mathcal{Q}_{\mathcal{M}}\left(s_{N_t}^{\mathrm{SIC}}\right)$. By utilising this estimated value and considering the property of matrix $\mathbf{R}$, the previous element of $\mathbf{s}^{\mathrm{eq}}$ can be obtained by $s_{N_t-1}^{\mathrm{SIC}} = \left(v_{N_t-1} - R_{N_t-1,N_t}\hat{s}_{N_t}^{\mathrm{SIC}}\right)/R_{N_t-1,N_t-1}$. Thereby, the SIC detection is possible to be achieved sequentially, and the $n$th estimation of it is

$$\hat{s}_n^{\mathrm{SIC}} = \mathcal{Q}_{\mathcal{M}}\left(\frac{v_n - \sum_{i=n+1}^{N_t} R_{n,i}\hat{s}_i^{\mathrm{SIC}}}{R_{n,n}}\right). \tag{4}$$

### *B. LR-aided Detectors*

To restore the full receive diversity order $N_r$, the LR technique is applied to the detection. The channel matrix $\mathbf{H}$ can be treated as a lattice basis and each column of $\mathbf{H}$ represents a basis vector. The target of LR is to find a basis that not only supports the same lattice but also has shorter and nearly orthogonal basis vectors. We denote the lattice reduced matrix as $\mathbf{H}_{\mathrm{LR}} = \mathbf{HT}$, where $\mathbf{T}$ is a complex integer unimodular matrix and $\mathbf{H}_{\mathrm{LR}}$ spans the same lattice as $\mathbf{H}$. Therefore, by substituting it into Equation (1) and introducing the transformed symbol $\mathbf{z} = \mathbf{T}^{-1}\mathbf{s}$, we have

$$\mathbf{y} = \mathbf{H}\mathbf{T}\mathbf{T}^{-1}\mathbf{s} + \mathbf{n} = \mathbf{H}_{\mathrm{LR}}\mathbf{z} + \mathbf{n}. \tag{5}$$

Consequently, instead of retrieving the transmitted symbol $\mathbf{s}$ directly, an intermediate step can be performed. Clearly, an estimated value $\hat{\mathbf{z}}$ can be achieved from $\mathbf{y}$ first. Then, by left-multiplying $\mathbf{T}$ to $\hat{\mathbf{z}}$, the estimation of $\mathbf{s}$ is obtained. This provides the primal procedure of the LR-aided detection. If the constellation set of the transmitted symbol $\mathbf{s}$ is the infinite complex integer plane, then the lattice reduced constellation set in the z-domain consists of the infinite complex integer plane as well. And this basic procedure is applicable. However, the square $M$-ary quadrature amplitude modulation (QAM) is often applied to the MIMO system, which forms a finite lattice excluding the origin point. Therefore, the original constellation must be scaled and shifted such that the detection can be conducted on a consecutive complex integer lattice. Let $\mathcal{M}$ denote the finite QAM set, thus $\mathbf{s} \in \mathcal{M}^{N_t}$, and the scaled and shifted transmitted symbol is defined as

$$\tilde{\mathbf{s}} = \frac{1}{\alpha}\mathbf{s} + \frac{1}{2}\mathbf{1}_c, \tag{6}$$

where $\alpha$ is the minimum Euclidean distance between two constellation points in set $\mathcal{M}$ and $\mathbf{1}_c$ is an $N_t \times 1$ vector whose entries have the same value $(1+j)$. By substituting Equation (6) into (1), the translated received signal is given as

$$\tilde{\mathbf{y}} = \frac{1}{\alpha}\mathbf{y} + \frac{1}{2}\mathbf{H}\mathbf{1}_c = \mathbf{H}\tilde{\mathbf{s}} + \tilde{\mathbf{n}}, \tag{7}$$

where $\tilde{\mathbf{n}} = \frac{1}{\alpha}\mathbf{n}$. Hence, similar to Equation (5), the lattice reduced system model based on the scaled and shifted expression can be represented as $\tilde{\mathbf{y}} = \mathbf{H}_{\mathrm{LR}}\tilde{\mathbf{z}} + \tilde{\mathbf{n}}$, where $\tilde{\mathbf{z}} = \mathbf{T}^{-1}\tilde{\mathbf{s}}$. Thus, we can conduct detections on this modified model.

For the LR-aided linear detection, the equalised value can be computed by $\tilde{\mathbf{z}}^{\mathrm{eq}} = \mathbf{H}_{\mathrm{LR}}^{\dagger}\tilde{\mathbf{y}}$. As the columns of $\mathbf{H}_{\mathrm{LR}}$ are roughly orthogonal, the noise amplified by it is much less than the one in Equation (2). Therefore, the reliability of quantisation on symbol $\tilde{\mathbf{z}}^{\mathrm{eq}}$ is higher than on the symbol $\mathbf{s}^{\mathrm{eq}}$. And by using (7), $\tilde{\mathbf{z}}^{\mathrm{eq}}$ can be expressed as

$$\tilde{\mathbf{z}}^{\mathrm{eq}} = \frac{1}{\alpha}\mathbf{H}_{\mathrm{LR}}^{\dagger}\mathbf{y} + \frac{1}{2}\mathbf{T}^{-1}\mathbf{1}_c. \tag{8}$$

Now, the remaining part is to retrieve the original transmitted symbol $\mathbf{s}$ from $\tilde{\mathbf{z}}^{\mathrm{eq}}$. As the estimation of $\tilde{\mathbf{z}}^{\mathrm{eq}}$ is in the $\tilde{z}$-domain, each element of this vector must be quantised to the feasible constellation point of $\tilde{\mathbf{z}}$. The simplest solution (although suboptimal) is to replace this constrained quantisation by an element-wise integer-rounding operation to get the estimation of $\tilde{\mathbf{z}}^{\mathrm{eq}}$ first, then transform this rounded vector to the $s$-domain and use the function $\mathcal{Q}_{\mathcal{M}}$ to recover the original transmitted symbol. Hence, by substituting $\tilde{\mathbf{z}} = \mathbf{T}^{-1}\tilde{\mathbf{s}}$ into Equation (6), the estimation of the original symbol $\mathbf{s}$ is given by

$$\hat{\mathbf{s}}^{\mathrm{eq}} = \mathcal{Q}_{\mathcal{M}}\left(\alpha\mathbf{T}\lfloor\tilde{\mathbf{z}}^{\mathrm{eq}}\rceil - \frac{\alpha}{2}\mathbf{1}_c\right), \tag{9}$$

where $\lfloor\cdot\rceil$ represents the nearest integer rounding function which rounds the input element to the nearest integer. For complex inputs, it treats the real and imaginary parts individually.

Apparently, the LR can be integrated with SIC detection either. Let the QR decomposition of the lattice reduced channel matrix be $\mathbf{H}_{\mathrm{LR}} = \mathbf{Q}_{\mathrm{LR}}\mathbf{R}_{\mathrm{LR}}$, and then we can obtain $\mathbf{R}_{\mathrm{LR}}\tilde{\mathbf{z}}^{\mathrm{eq}} = \mathbf{Q}_{\mathrm{LR}}^{\mathcal{H}}\tilde{\mathbf{y}}$. By substituting (7), we have

$$\mathbf{R}_{\mathrm{LR}}\tilde{\mathbf{z}}^{\mathrm{eq}} = \frac{1}{\alpha}\mathbf{Q}_{\mathrm{LR}}^{\mathcal{H}}\mathbf{y} + \frac{1}{2}\mathbf{R}_{\mathrm{LR}}\mathbf{T}^{-1}\mathbf{1}_c = \mathbf{u}, \tag{10}$$

which has the same structure as Equation (3). Thus, the estimation of $\tilde{\mathbf{z}}^{\mathrm{eq}}$ can also be obtained successively. The only difference is that the quantisation function $\mathcal{Q}_{\mathcal{M}}$ in Equation (4) has to be replaced by the integer rounding function. Thereby, the $n$th element of the estimation $\widehat{\tilde{\mathbf{z}}}^{\,\mathrm{SIC}}$ is

$$\widehat{\tilde{z}}_{\,n}^{\,\mathrm{SIC}} = \left\lfloor \frac{u_n - \sum_{i=n+1}^{N_t} R_{n,i}^{\mathrm{LR}}\,\widehat{\tilde{z}}_{\,i}^{\,\mathrm{SIC}}}{R_{n,n}^{\mathrm{LR}}} \right\rceil, \tag{11}$$

where $R_{n,i}^{\mathrm{LR}}$ represents the $(n,i)$th entry of the upper triangular matrix $\mathbf{R}_{\mathrm{LR}}$. Finally, the estimation of the original signal in the s-domain is determined by

$$\hat{\mathbf{s}}^{\mathrm{SIC}} = \mathcal{Q}_{\mathcal{M}}\left(\alpha\mathbf{T}\widehat{\tilde{\mathbf{z}}}^{\,\mathrm{SIC}} - \frac{\alpha}{2}\mathbf{1}_c\right), \tag{12}$$

which completes the LR-aided SIC detection. It is worth mentioning that the sorted QR (SQR) decomposition can be applied to $\mathbf{H}_{\mathrm{LR}}$ to provide an $\mathbf{R}_{\mathrm{LR}}$ with optimal diagonal ordering, thus, improves the SIC detection performance. This motivates us to implement SQR to the SIC detection throughout this paper.

### C. LLL and SA Reduction

Theoretically, the complexity of finding an optimal basis for a lattice is quite high. To reduce the complexity and make it feasible for the practical problem, some suboptimal solutions are proposed. Among them, LLL and SA are adopted here as the former is widely used and the latter is considered as an alternative.

It is well known that a basis is called LLL reduced if it satisfies two conditions: *size reduced condition* and *Lovász condition*. However, this definition is proposed for the real domain. As the channel matrix $\mathbf{H}$ usually has complex entries, a complex LLL (CLLL) which can operate directly on complex bases is of great interest. To further reduce the complexity, the Siegel condition in [32] is adopted to replace the Lovász condition. Thus, a CLLL variant is obtained by definition: An $M \times N$ matrix $\mathbf{H} = \mathbf{QR}$ is Siegel-CLLL reduced if it satisfies the following two conditions,

- *complex size reduced condition*

$$|\Re\left(R_{l,k}\right)| \leq \frac{1}{2}|R_{l,l}| \quad \text{and} \quad |\Im\left(R_{l,k}\right)| \leq \frac{1}{2}|R_{l,l}|, \quad \forall\ 1 \leq l < k \leq M; \tag{13}$$

- *Siegel condition*

$$|R_{k-1,k-1}|^2 \leq \zeta |R_{k,k}|^2, \quad \forall\ k = 2, \ldots, M, \tag{14}$$

where parameter $\zeta$ is chosen from the interval $[2, 4]$. This CLLL variant is used for all the experiments throughout this paper with $\zeta = 2$. By checking the algorithm in [33], one can find that the process of each iteration can be divided into two parts, *size reduction* and *basis update*. For each loop, the size reduction should be conducted first and the Siegel condition will be evaluated subsequently. If the Siegel condition is satisfied, the algorithm continues with the next iteration. Otherwise, the basis update process has to be performed. Clearly, the complexity of this algorithm highly depends on this step. Not only because it requires the column swapping and matrix multiplication, but also owing to the counter decreasing caused by it.

Unlike the LLL algorithm which only aims at finding a near-orthogonal basis for the lattice spanned by the original basis (channel matrix in this article), SA optimises this lattice together with its dual lattice. Let an $M \times N$ matrix $\mathbf{H} = [\mathbf{h}_1, \mathbf{h}_2, ..., \mathbf{h}_N]$ denote a basis which spans a lattice $\mathcal{L}$, then the basis which spans the dual lattice of $\mathcal{L}$ can be defined as $\mathbf{H}^* = \left(\mathbf{H}^\dagger\right)^T = [\mathbf{h}_1^*, \mathbf{h}_2^*, ..., \mathbf{h}_N^*]$. The Seysen's metric is utilised to assess the orthogonality of a basis $\mathbf{H}$, which is

$$S\left(\mathbf{H}\right) = \sum_{n=1}^{N} \|\mathbf{h}_n\|^2 \|\mathbf{h}_n^*\|^2. \tag{15}$$

It is known that $S\left(\mathbf{H}\right) \geq N$ and when $\mathbf{H}$ is an orthogonal matrix, equality holds. Thus, SA performs a basis update on $\mathbf{H}$ iteratively until the Seysen's metric of the updated basis cannot be further reduced. Based on the different criterion of choosing the basis vector which needs to be updated, two approaches, lazy implementation and greedy implementation, are proposed. In this paper, we focus on the latter as it is more efficient in complexity and convergence speed [8], [34]. The detailed algorithm can be found in [29].

## III. Proposed Algorithms

In this section, we propose algorithms applying SA to ILR. First of all, the feasibility of adopting SA to ILR is analysed. Subsequently, we propose a sorted QR based SA algorithm. Finally, by merging this algorithm with the SIC detector properly, an SA-aided ILR algorithm is introduced.

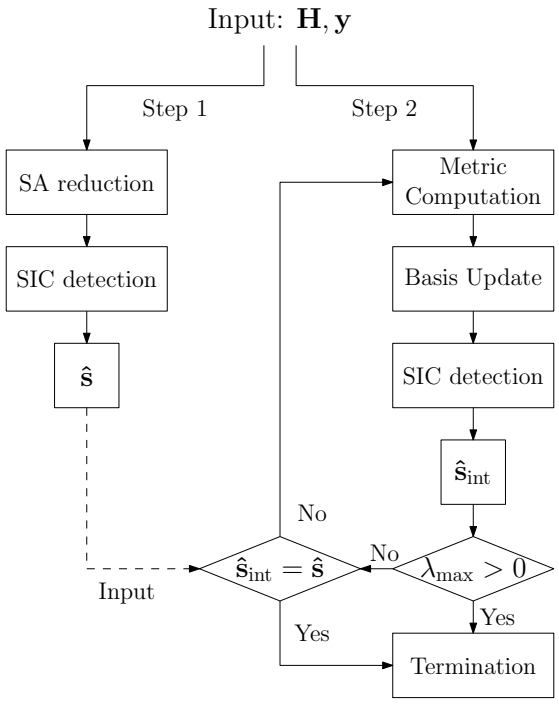


Fig. 1: The flow chart for finding the ideal ET of SA.

### *A. Feasibility Discussion*

ILR is a technique which can jointly optimise the LR and the detection process of a system while maintaining the full diversity. The original ILR is introduced in [23], which first obtains the estimated symbol by conducting a SIC detection on the partially reduced channel matrix that has to be updated at each CLLL iteration, then employs an ET scheme to stop the process.

Obviously, ET is the crucial step for reducing the complexity of the ILR algorithm. As the name describes, ET refers to the methods that can terminate the LR process in advance while still preserving the same or almost the same performance. However, most ET techniques only focus on terminating the LR algorithm according to the channel characteristics [19], [21], [22]. The detection process has rarely been taken into consideration. Intuitively, the LR process can be terminated if the detector can retrieve the transmitted symbol correctly based on the partially reduced channel matrix. Therefore, ILR conducts ET based on an RA [24]. Let $\hat{\mathbf{s}}_{\text{int}}$ denote the estimated symbol which is obtained from the intermediate values ($\mathbf{Q}$, $\mathbf{R}$ and $\mathbf{T}$) in the LR process, and the RA is expressed as

$$\|\bar{\mathbf{y}} - \bar{\mathbf{H}}\hat{\mathbf{s}}_{\text{int}}\| \leq \gamma \frac{\sigma_n}{\sqrt{N_t}}, \tag{16}$$

where the constant $\gamma \geq 0$ is a threshold parameter. If the condition in (16) is satisfied by an estimation $\hat{\mathbf{s}}_{\text{int}}$, this vector will be used as the final estimation, and the remaining iterations of CLLL will not be executed.

As the SA based linear detector outperforms the CLLL based one [34], an ILR algorithm with SA is of great interest. Before adopting SA to the ILR, we have to validate that it is feasible to terminate the SA during its execution process while the detector can still provide the same performance with the intermediate parameters. Thus, an experiment is conducted to prove it and an optimal ET bound is achieved in the meantime. The flow chart for finding the ideal ET of SA is given in Figure 1. For each iteration, we first obtain the ideal estimation $\hat{\mathbf{s}}^{\text{LR}}$ based on the original SA, see Step 1 in Figure 1. Then, in the same iteration, another SA is applied to the initial inputs as Step 2. The difference is that whenever there is an update of the channel matrix during the execution of the second SA, a detection must be made to

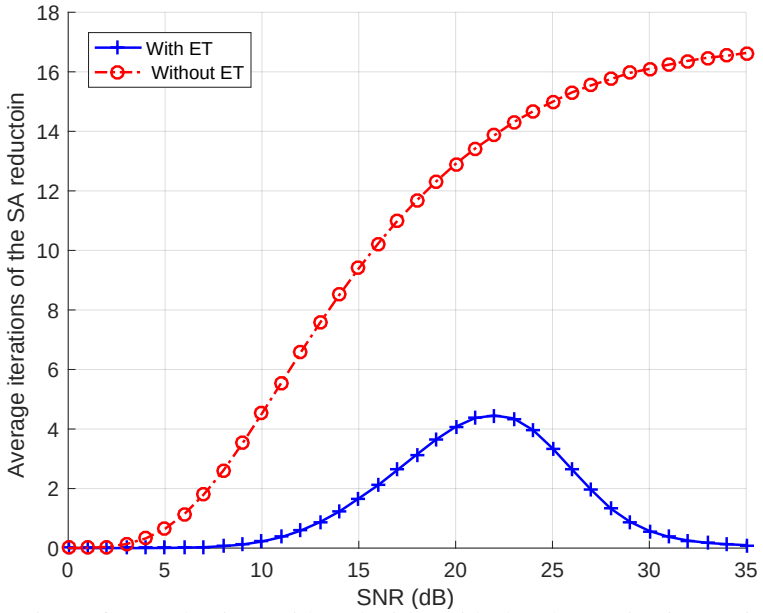


Fig. 2: The average iterations of SA reductions with and without ideal early termination against SNR for a 64-QAM $8 \times 8$ MIMO system in a spatial uncorrelated channel.

acquire an intermediate estimation $\hat{\mathbf{s}}_{\text{int}}^{\text{LR}}$ from the current channel matrix. Further, if $\hat{\mathbf{s}}_{\text{int}}^{\text{LR}} = \hat{\mathbf{s}}^{\text{LR}}$, the second SA process stops. This gives us the optimal ET.

We conduct a simulation on an $8 \times 8$ MIMO system with 64-QAM under the uncorrelated Rayleigh fading channel and apply the SA to the augmented channel matrix $\mathbf{H}$ in the extended system (recall that this system facilitates MMSE based detections). The average iterations of an SA reduction with and without ideal ET against SNR are shown in Figure 2. Obviously, the number of the average iterations for one LR process is reduced dramatically by introducing ET into the system. The iterations of the conventional SA keeps increasing and has a trend to converge at 17 times per reduction from the point SNR $\geq 35$ dB. On the other side, the number of iterations of ET-injected SA increases later and slower. This holds as the SA cannot benefit the SIC detection significantly in the lower SNR range (from 0 dB to 10 dB) as Gaussian noise is the main cause of errors. Consequently, it is unnecessary to conduct the SA reductions in most instances, which results in a very small number of average iterations of the ideal ET based SA. With the increase of the SNR, the influence of the Gaussian noise reduces, the SA reduction starts to function and improves the SIC detection. Hence, the average iterations of the ET-aided SA keeps growing and reaches the maximum around 4.5 iterations per reduction with SNR $= 23$ dB. Afterwards, this value starts to decrease and becomes nearly 0 at SNR $= 35$. The reason for this decreasing is that as SNR grows, an increasing number of accurate estimations can be obtained based on the partial SA reduction with less iterations. Even in some cases, the SA reduction can be totally discarded as the pure SIC detector can retrieve the correct transmitted symbol directly. Overall, the ET is not only feasible but also benefits the system significantly, especially in the higher SNR range. It is worth noting that the ideal ET carried out in this simulation does not reduce the BER performance of the SA based SIC detection at all. In fact, recalling that the termination only happens at the point when the intermediate estimation is equal to the original estimation obtained from the SA without ET, i.e., $\hat{\mathbf{s}}_{\text{int}}^{\text{LR}} = \hat{\mathbf{s}}^{\text{LR}}$, the BER performance of the SA based SIC with and without ideal ET are exactly the same.

### *B. Sorted QR based SA*

As discussed above, the SIC detection has to be conducted in the intermediate step of an LR process to accomplish the ILR, which means the corresponding orthogonal matrix $\mathbf{Q}$ and upper triangular matrix $\mathbf{R}$ of the partially reduced channel matrix must be obtained. Conventionally, the SA is realised by updating

the channel matrix $\mathbf{H}$ directly. Thus, an extra QR decomposition is required for each intermediate SIC detection, which is absolutely impractical as it increases the complexity of the SA dramatically.

Therefore, an alternative algorithm called SQR-SA is proposed here to avoid this. It utilises the SQR to obtain the initial matrices $\mathbf{Q}$ and $\mathbf{R}$ from the original channel matrix $\mathbf{H}$ first, then updates $\mathbf{Q}$ and $\mathbf{R}$ iteratively to complete the SA reduction. The detailed algorithm is presented in Algorithm I. Generally, after the SQR and initialisation (Line 1-2), each iteration of this algorithm consists of two main parts, *Seysen's metric computation* and *basis update*. Furthermore, the latter can be partitioned into two steps, the matrix update and the triangularization.

Algorithm I: Sorted QR based SA

**Input:** $\mathbf{H}$
**Output:** $\mathbf{Q}, \mathbf{R}, \mathbf{T}$
1: $[\mathbf{Q}, \mathbf{R}, \mathbf{T}] = \text{Sorted\_QR}(\mathbf{H})$
2: $\mathbf{G} = \mathbf{R}^H\mathbf{R},\ \mathbf{G}^{-1},\ ite = 1,\ \lambda_{\max} = 1$
3: **while** $\lambda_{\max} > 0$ **do**
4: **if** $ite == 1$ **then**
5: **for** $i, j = 1$ to $N_t$, and $i \neq j$ **do**
6: $\lambda_{i,j} = \lfloor x_{i,j} \rceil$ with $x_{i,j} = \frac{1}{2}\left(\frac{G^{-1}_{j,i}}{G^{-1}_{i,i}} - \frac{G_{j,i}}{G_{j,j}}\right)$
7: $\Delta_{i,j} = 2G_{j,j}G^{-1}_{i,i}\left(2\Re(\lambda^*_{i,j}x_{i,j}) - |\lambda_{i,j}|^2\right)$
8: **end for**
9: $ite = 0$
10: **else**
11: **for** $i, j = 1$ to $N_t$, with $i \neq s$ , $j \neq t$ **do**
12: update $\lambda$ and $\Delta$ with index pairs $(i, s), (j, t), (s, i)$ and $(t, j)$ according to Line 6 and 7, respectively.
13: **end for**
14: **end if**
15: $\lambda_{\max} = \max(|\lambda|)$
16: $(s, t) = \arg\max_{(i,j)} \Delta$
17: **if** $\lambda_{\max} > 0$ **then**
18: $G_{s,k} = G_{s,k} + \lambda^*_{s,t}G_{t,k},\ \ G_{k,s} = G^*_{s,k},\ \ k \neq s$
19: $G_{s,s} = G_{s,s} + 2\Re(\lambda^*_{s,t}G_{t,s}) + |\lambda^*_{s,t}|^2G_{t,t}$
20: $G^{-1}_{t,k} = G_{t,k} - \lambda_{s,t}G^{-1}_{s,k},\ \ G^{-1}_{k,t} = (G^{-1}_{t,k})^*,\ \ k \neq t$
21: $G^{-1}_{t,t} = G^{-1}_{t,t} - 2\Re(\lambda_{s,t}G^{-1}_{t,s}) + |\lambda_{s,t}|^2G_{s,s}$
22: $\boldsymbol{R}_{:,s} = \boldsymbol{R}_{:,s} + \lambda_{s,t}\boldsymbol{R}_{:,t}$
23: $\boldsymbol{T}_{:,s} = \boldsymbol{T}_{:,s} + \lambda_{s,t}\boldsymbol{T}_{:,t}$
24: **if** $s < t$ **then**
25: **for** $m = s : t - 1$ **do**
26: **if** $m == s$ **then**
27: $tt = t$
28: **else**
29: $tt = m + 1$
30: **end if**
31: **for** $n = tt : -1 : m + 1$ **do**
32: $\boldsymbol{\Theta} = \frac{1}{\|\boldsymbol{R}_{n-1:n,m}\|}\begin{bmatrix} R^*_{n-1,m} & R^*_{n,m} \\ -R_{n,m} & R_{n-1,m} \end{bmatrix}$
33: $\boldsymbol{R}_{n-1:n,m:\text{end}} = \boldsymbol{\Theta}\boldsymbol{R}_{n-1:n,m:\text{end}}$
34: $\boldsymbol{Q}_{:,n-1:n} = \boldsymbol{Q}_{:,n-1:n}\boldsymbol{\Theta}^{\mathcal{H}}$
35: **end for**
36: **end for**
37: **end if**
38: **end if**
39: **end while**

| | | | |
|---|---|---|---|
| Metric Computation | : line 4-16 | | |
| Basis Update | : line 17-38 | Matrix Update | (line 18-23) |
| | | Triangularization | (line 24-37) |

In the Seysen's metric computation part, all update parameters $\lambda_{i,j}$ and their corresponding decrease

on the Seysen's metric $\Delta_{i,j}$ must be initialised at the first iteration (Line 4-9). In the following iterations, $\lambda_{i,j}$ and $\Delta_{i,j}$ can be updated partially (Line 10-14). Afterwards, we have to find the maximum absolute value $\lambda_{\max}$ over all update parameters $\lambda_{i,j}$ (Line 15) and obtain the indices $(s,t)$ of the update parameter which can offer the maximum decrease on the Seysen's metric (Line 16). In addition, the indices pair $(s,t)$ and their corresponding update parameter $\lambda_{s,t}$ are utilised for updating the basis in the following part.

Considering that the target of the SA reduction is to minimise the Seysen's metric given in (15), which can be equivalently transferred to render all the update parameters $\lambda$ to 0 [29], thus, for the greedy approach, the basis update part aims at reducing the basis with the update parameter whose indices can provide the maximum decrease on the Seysen's metric, i.e., $\lambda_{s,t}$. Apparently, the condition of entering the basis update part is $\lambda_{\max} > 0$. From Line 18-23, the Gram matrix $\mathbf{G}$, its inverse $\mathbf{G}^{-1}$, the triangular matrix $\mathbf{R}$ and the mapping matrix $\mathbf{T}$ are updated according to their updating rules with parameter $\lambda_{s,t}$, respectively. However, the update on $\mathbf{R}$ may destroy the upper triangularity of it. For example, if the 4$^{\text{th}}$ column of $\mathbf{R}$ is added to the 2$^{\text{nd}}$ column, the entries $R_{4,2}$ and $R_{3,2}$ are not zeros any more. Therefore, when $s < t$, the process triangularization must be conducted to recover this property of $\mathbf{R}$ (Line 24-37). In particular, the Givens rotation is applied recursively to null these undesirable entries and make the diagonal elements of $\mathbf{R}$ real and positive again. Further, the orthogonal matrix $\mathbf{Q}$ has to be updated correspondingly to make the multiplication of $\mathbf{QR}$ unchanged. And matrix $\mathbf{\Theta}$ in line 32 is the Givens rotation matrix. After the basis update part, the SQR-SA algorithm enters the metric computation part in the next iteration (Line 11-13), which renders the values of $\lambda_{s,t}$ and $\Delta_{s,t}$ to 0.

### *C. SA based ILR*

From the previous discussion, we learn that the SA reduction can be realised by updating $\mathbf{Q}$ and $\mathbf{R}$ iteratively. This property ensures that the SIC detection can be integrated with SQR-SA at each iteration without conducting an extra QR decomposition. Thus, we can terminate the SA process based on the estimations obtained from the SIC detector, according to the RA criterion, which underlays the SA based ILR. To realise this algorithm, the RA in Equation (16) must be extended to the $z$-domain, which is

$$\left\|\mathbf{Q}^{\mathcal{H}}\tilde{\mathbf{y}} - \mathbf{R}\tilde{\mathbf{z}}\right\|^2 \leq \frac{1}{N_t}\left(\frac{\gamma\sigma_n}{\alpha}\right)^2. \tag{17}$$

Intuitively, the complexity of this algorithm is very high if we perform a SIC detection at each iteration. Therefore, some useful properties are applied to reduce the complexity.

First, there are two processes, i.e., matrix update and triangularization, in the basis update part of the SA-ILR. If only the matrix update is carried out (when $\geq t$), then the estimations obtained from the SIC detector are the same before and after this process. Hence, there is no need to conduct the SIC detection as the estimation is identical to the one in the last iteration. On the other hand, if a triangularization process appears (when $s < t$), then part of the matrix $\mathbf{R}$ is reconstructed, which leads to a change in the result of the SIC detection. In this case, the SIC must be conducted. Overall, considering that we just need to conduct SIC detection after a triangularization process, the complexity can be reduced significantly by applying this into the algorithm.

Second, by scrutinising the triangularization procedure, one can conclude that the SIC and RA only need to be partially recalculated. When the $s^{\text{th}}$ column of $\mathbf{R}$ is updated by the $t^{\text{th}}$ column vector (recall $s < t$ in this case), after the triangularization process, the $(t+1)^{\text{th}}$ to $N_t{}^{\text{th}}$ row vectors of $\mathbf{R}$ stay the same, as well as the entries with the corresponding indices of vector $\mathbf{u}$. By revisiting Equation (10) and (11), we see that the estimations with indices larger than $t$ do not change. Therefore, the entries need to be recomputed for the SIC, and RA steps are reduced.

Based on these properties, we propose the algorithm SA-ILR which is presented in Algorithm II. In general, it can be divided into three parts, *partial computation*, *constrained termination* and *SA reduction*. In the first part, the SIC detection and RA are partially recalculated according to the previous description

and this process is ended if the RA criterion is not satisfied (see Line 5-15). Afterwards, we enter the constrained termination part. If the termination requirement is fulfilled, this process will be activated. The constraint $\hat{\mathbf{s}} == \left(\alpha\mathbf{Tz} - \frac{\alpha}{2}\mathbf{1}_c\right)$ in Line 17 of Algorithm II can improve the accuracy of the estimation as it eliminates the demodulation error caused by $\mathcal{Q}_{\mathcal{M}}$. However, it also induces an increase in the complexity as additional iterations may be conducted to meet this constraint. Therefore, the tradeoff of this should be taken into consideration when using this algorithm. A discussion of the constrained and unconstrained terminations will be made based on numerical results in the next section. Finally, the algorithm enters the SA reduction part. It is quite similar to the algorithm SQR-SA except that two additional operations are included. One is the update of the corresponding vector $\mathbf{u}$ for SIC detection in the triangularization process, see line 24 in Algorithm II. The other one is to provide an evidence (the variable $flag$ in Algorithm II) of the triangularization to start the partial computation part.

It is worthy to point out that the SA-ILR may have a better BER performance than the SQR-SA based SIC detection. This is due to the fact that we may achieve a matrix $\mathbf{R}$ with better diagonal ordering during the SQR-SA process to facilitate a better SIC detection.

Algorithm II: SA based ILR

**Input:** $\mathbf{H}, \mathbf{y}, \varphi = \frac{1}{N_t}\left(\frac{\gamma\sigma_n}{\alpha}\right)^2$
**Output:** $\hat{\mathbf{s}}$

1: $[\mathbf{Q}, \mathbf{R}, \mathbf{T}] = \mathrm{Sorted\_QR}\,(\mathbf{H})$
2: $\mathbf{G} = \mathbf{R}^H\mathbf{R},\ \mathbf{G}^{-1},\ ite = 1,\ \lambda_{\max} = 1$
3: $\mathbf{u} = \frac{1}{\alpha}\left(\mathbf{Q}^{\mathcal{H}}\mathbf{y} + \mathbf{R}\mathbf{1}_c\right), l = N_t, \tau = N_t, flag = 1$
4: **while** TRUE **do**
5: **if** $flag == 1\ ||\ \lambda_{\max} == 0$ **then**
6: **for** $k = \tau : -1 : 1$ **do**
7: $\pi = u_k - \sum_{j=k+1}^{N_t} R_{k,j} z_j$
8: $z_k = \lfloor \pi / R_{k,k} \rceil$
9: $l = k$
10: **if** $\varphi > 0$ **then**
11: $a_k = a_{k+1} + |\pi - R_{k,k} z_k|^2$
12: **if** $a_k > \varphi \rightarrow$ break
13: **end if**
14: **end for**
15: **if** $a_l \leq \varphi\ ||\ \lambda_{\max} == 0$ **then**
16: $\hat{\mathbf{s}} = \mathcal{Q}_{\mathcal{M}}\left(\alpha\mathbf{Tz} - \frac{\alpha}{2}\mathbf{1}_c\right)$
17: **if** $\hat{\mathbf{s}} == \left(\alpha\mathbf{Tz} - \frac{\alpha}{2}\mathbf{1}_c\right)\ ||\ \lambda_{\max} == 0 \rightarrow$ break
18: **end if**
19: **end if**
20: Metric Computation (Line 4-12 in Algorithm I)
21: **if** $\lambda_{\max} > 0$ **then**
22: Matrix Update (Line 14-19 in Algorithm I)
23: **if** $s < t$ **then**
24: Modified Triangularization (Take line 21-32 in Algorithm I and add $\mathbf{u}_{n-1:n} = \mathbf{\Theta}\mathbf{u}_{n-1:n}$ after line 30.)
25: $\tau = \max(l, t)$
26: $flag = 1$
27: **else**
28: $flag = 0$
29: **end if**
30: $\Delta_{\max} = 0$
31: **end if**
32: **end while**

| | | | |
|---|---|---|---|
| Partial Computation | : line 6-14 | | |
| Constrained Termination | : line 15-18 | | |
| SA Reduction | : line 20-31 | Metric Computation | (line 20) |
| | | Matrix Update | (line 22) |
| | | Modified Triangularization | (line 24) |

### D. Analytical Computational Complexity

As we know, the computational complexity of an algorithm is vital in a communication system, especially for the detection part at the receiver side. Thus, we analyse the complexity of the proposed SA-ILR algorithm in this subsection. The floating point operations (FLOPs) are employed here as the metric to evaluate the computation complexity. Note that one FLOP represents a complex summation or a complex multiplication here.

By sifting through Algorithm II, one can observe that the exact complexity of the SA-ILR is determined by the required iterations of its five parts, i.e., partial computation, constrained termination, metric computation, matrix update and modified triangularization. We assume that the total iterations of these parts are $L_1, L_2, ..., L_5$, respectively. Therefore, the overall FLOPs of the algorithm in the worst case can be calculated by

$$\begin{aligned} &L_1(N_t^2+6N_t)+L_2(2N_t^2+2N_t)+L_4(20N_t-16) \\ &\quad+\left[12(Nt-1)^2+(L_3-1)48(N_t-1)\right]+L_5(6N_r+6N_t+1). \end{aligned} \tag{18}$$

In addition, to simplify Equation (18), the corresponding asymptotic expression of the SA-ILR can be achieved as $\mathcal{O}\big((L_1+2L_2+12)N_t^2\big)$, while the asymptotic expression of the CLLL-ILR is $\mathcal{O}\big((L_1+2L_2)N_t^2\big)$. Note that the values of $L_1$ and $L_2$ in CLLL-ILR are different from their values in the case of SA-ILR. Furthermore, according to these asymptotic expressions, it is easy to conclude that the partial computation and constrained termination parts contribute most to the complexities of both methods.

On the other hand, apart from the iteration numbers, the most significant difference between the two algorithms is that the initialisation (Line 5-8 in Algorithm I) of the metric computation part for the SA-ILR brings additional $\mathcal{O}\big(12N_t^2\big)$ FLOPs. However, this extra calculation will vanish when $L_3$ is 0. In this case, the SA-ILR only executes the partial computation and the constrained termination parts in the first iteration, and ends before entering the SA reduction part (Line 20-31 in Algorithm I). Thus, the total iteration of the out loop, $L_1$ and $L_2$ are all equal to 1. Consequently, the SA-ILR degrades to a pure SIC detector. It is worth mentioning that this pure SIC detector usually exhibits a comparable performance to the SA based one as the ET condition ($a_l \leq \varphi$ in Line 15 of Algorithm I) must be satisfied. Moreover, the same degradation to the pure SIC detector applies to the CLLL-ILR algorithm as well, which makes the complexity of SA-ILR and CLLL-ILR equal in this situation. Therefore, the complexity of SA-ILR is not always $\mathcal{O}\big(12N_t^2\big)$ higher than that of CLLL-ILR. More importantly, this property ensures that the two have relatively close complexity in the high SNR range, which will be validated in the following simulation section. Overall, the complexity orders of both two algorithms are the same, i.e., $\mathcal{O}\big(N_t^2\big)$.

## IV. Simulation and discussion

In this section, we provide our simulation results to evaluate the proposed SA based algorithms under both spatial uncorrelated and correlated channels. First, Section IV-A provides results validating the reliability and effectiveness of the SQR-SA scheme. Afterwards, in Section IV-B, we evaluate the influence of the early terminations parameter $\gamma$ on the performance of the BER and the complexity for the ILR schemes. Finally, a detailed and in-depth comparison between the proposed SA-ILR scheme and the LLL-ILR approach is provided in Section IV-C.

In these simulations, both the spatial uncorrelated channel (also known as canonical channel) and the correlated channel are considered. For the former, each entry of its channel matrix $\mathbf{H}$ is an i.i.d complex Gaussian distributed variable with zero mean and unit variance. As for the latter, by assuming the correlation between the receiving antennas and that between the transmitting antennas are independent, the channel matrix of the spatial correlated model can be obtained from [11], [35]. Note that the antenna array considered in this correlated model is the uniform linear array (ULA). Therefore, based on the type of channels, two different simulation scenarios are considered and their corresponding settings are given in Table I. Moreover, if not specified, the MMSE criterion is employed to all detection algorithms in the following.

Table I: Simulation parameters

| Parameters | Notation | Values | |
|---|---|---|---|
| | | Uncorrelated scenario | Correlated scenario |
| MIMO size | $N_t \times N_r$ | $8 \times 8$ | $64 \times 64$ |
| Modulation | $M$ | 64-QAM | 16-QAM |
| Spatial correlation index | $\rho$ | 0 | 0.2 |
| RA constant | $\gamma$ | Fixed, Optimal | Optimal |

### *A. SQR-SA Verification*

First of all, the proposed SQR-SA must be verified by comparing with the SQR-CLLL [23] in a scenario with uncorrelated channels. Note that the Siegel condition is employed in this SQR-CLLL algorithm. And the algorithm parameter $\zeta = 2.0$ utilised in the original SQR-CLLL is adapted to our simulations as well. Meanwhile, we have to demonstrate that the SQR-SA has comparable performance as the original SA. Therefore, a simulation of the conventional SA based SIC (SA-SIC) is introduced to the simulation as well, which applies an SQR decomposition to the SA reduced channel matrix at the end of the SA to accomplish the SIC detection. The performance of the SA-SIC can also provide the lower bound for the SA scheme. Finally, the plain SIC without LR is also included to show the baseline of the detection.

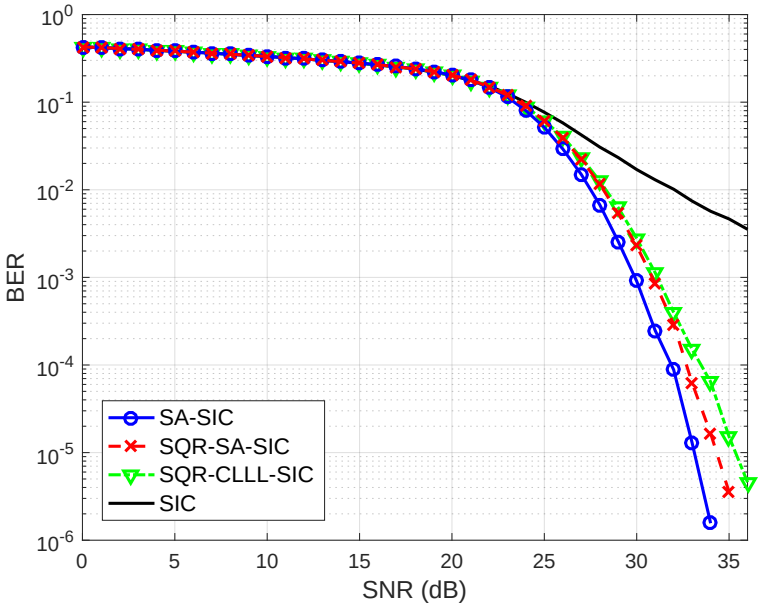


Fig. 3: The BER performance of the conventional SIC detection and different LR-aided SIC detections against SNR for a 64-QAM $8 \times 8$ MIMO system under a spatial uncorrelated channel.

The simulation result is given in Figure 3. As we can see from the plots, all the LR-aided SIC detectors outperform the plain SIC detector in the higher SNR range starting from 23 dB. Both two SA based SIC detections have a better performance than the CLLL aided one. Apparently, the SQR-SA-SIC does not have the same BER as the traditional SA-SIC. This is due to the fact that the latter performs the SQR at the final step, which provides a better-sorted $\mathbf{R}$ matrix to improve the SIC detection. However, if we want to conduct the SIC in the intermediate steps of the traditional SA to enable the ET, the complexity is greatly increased as extra SQR decomposition is required before each SIC detection. Hence, although the performance is slightly weakened by applying SQR-SA, it is still valuable as on the one hand it is better than the SQR-CLLL and on the other hand it plays an essential role in the SA-ILR algorithm.

### B. RA Constant $\gamma$

Obviously, in order to perform a successful ET, it is crucial to select a proper threshold parameter $\gamma$ for RA. If $\gamma$ is too small, the correct estimations are more likely not to satisfy the RA condition. And if $\gamma$ is set too big, the wrongly detected symbols have a higher chance to meet the RA requirement, thus to trigger the ET at the time. To study how this parameter $\gamma$ influences the BER performance and the complexity of ILR algorithms, we fix the SNR of the system and conduct simulations with a set of $\gamma$ values. In addition, recall that the constraint in line 17 of Algorithm II can be removed, therefore we have the constrained and unconstrained versions of the SA-ILR algorithm, as well as the CLLL-ILR algorithm. In the following, the impact of this constraint on the system performance against different $\gamma$ will also be investigated and discussed.

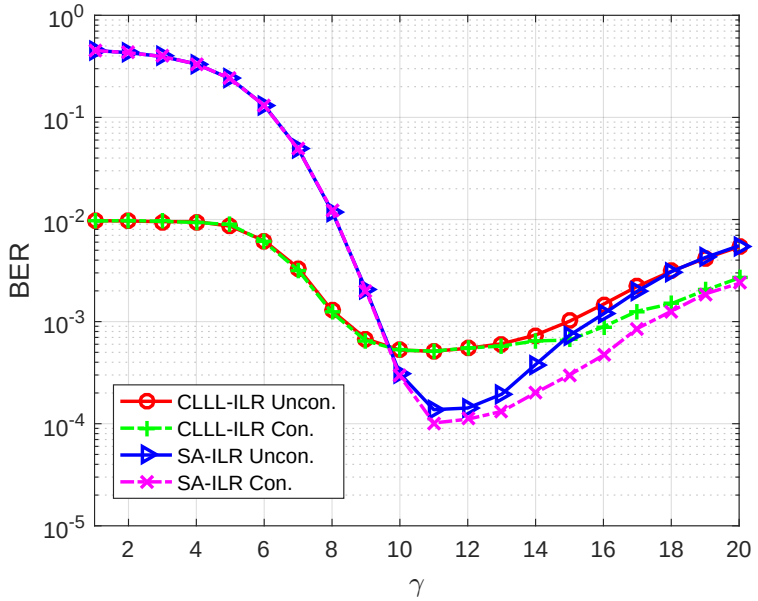


Fig. 4: The BER performance of ILR schemes against different $\gamma$ with SNR $= 32$ dB for a 64-QAM $8 \times 8$ MIMO system under a spatial uncorrelated channel.

*1) RA constant in uncorrelated scenario:* We first conduct simulations in the uncorrelated scenario with SNR $= 32$ dB. The plots of the BER against different RA parameters $\gamma$ for the four ILR algorithms are illustrated in Figure 4. In this case, all plots reach their optimal BER performance with parameter $\gamma = 11$ while the SA based algorithms have lower BERs. Intuitively, the SA-ILR algorithms are most obviously superior to the CLLL-ILR schemes when $\gamma \in [9, 14]$, which is called the feasible interval. We can see that this interval has a relatively broad range, which at least covers the optimal $\gamma$ for SNR from 27 dB to 36 dB (see the optimal $\gamma$ set in subsection IV-C2). Thus, an SNR degradation within a relatively wide range, i.e., 9 dB in this case, does not affect the system performance too much.

Generally, the SA based algorithms are more sensitive to the variation of $\gamma$. On the one hand, their performance degrades sharply when decreasing $\gamma$ from 11 to 1 and becomes much worse than the CLLL based algorithms with $\gamma \leq 9$. The reason is as follows. When $\gamma$ decreases in the interval $[1, 11]$, the termination condition becomes too tight, such that even if the correct symbol appears in the detection process, it still cannot satisfy the termination condition, thus, the algorithms carry on to process another symbol which makes the performance of the system even worse. On the other hand, increasing $\gamma$ from the optimal point 11 can also deteriorate the performance of the SA schemes. The reason is that, as $\gamma$ growth, the termination condition gets looser, which allows these algorithms to terminate easier before finding the correct symbol, hence, degrades the system performance. Finally, the introduction of the constraint can slow down the degradation trend for both SA and CLLL based algorithms and make the systems more robust to the deviation of the RA parameter $\gamma$.

Now, we analyse the relationship between the complexity and the RA constant $\gamma$. As discussed in Section III-D, the iterations of the partial computation and constrained termination parts, i.e., $L_1$ and $L_2$, contribute most to the complexity for both the SA-ILR and the CLLL-ILR schemes. Thus, we include these two parameters in our simulations. In addition, the average outer loop iterations are employed to help analyse the composition of complexity for each scheme. And we utilise the average FLOPs to evaluate the overall complexity of the proposed schemes.

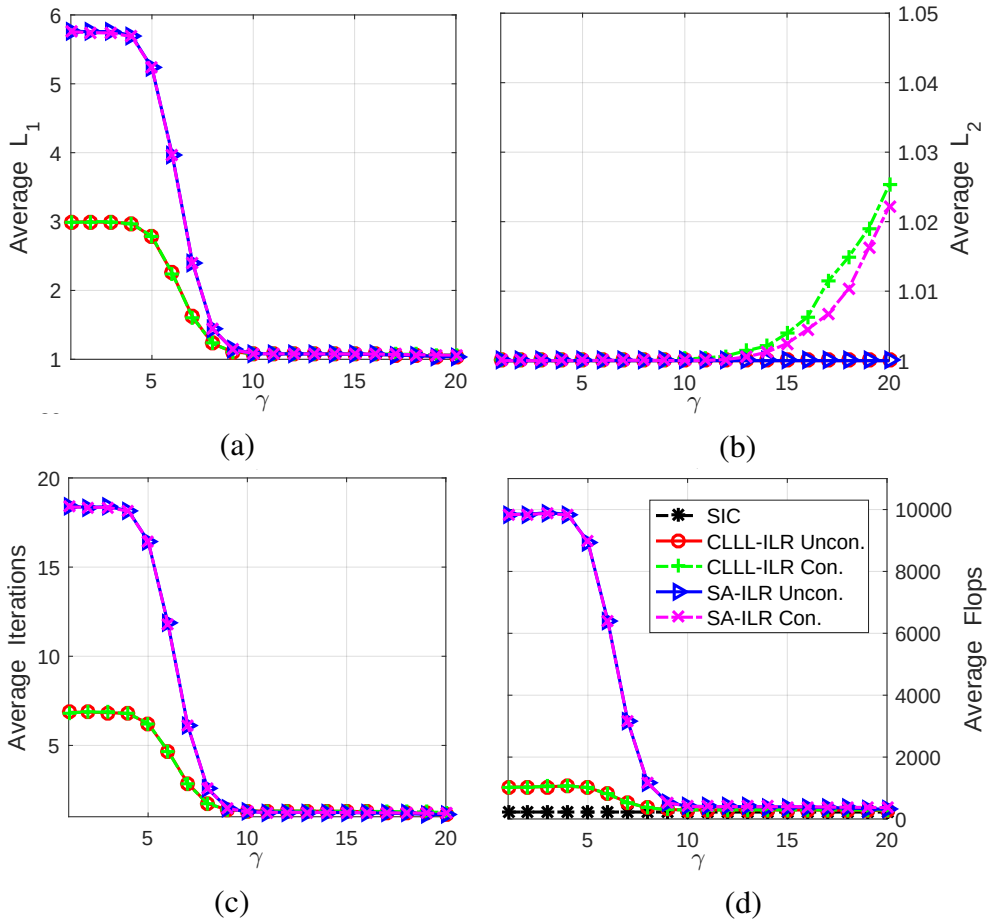


Fig. 5: The complexity parameters and FLOPs of ILR schemes against different $\gamma$ with SNR $= 32$ dB for a 64-QAM $8 \times 8$ MIMO system under a spatial uncorrelated channel.

The simulation results of these complexity parameters against different $\gamma$ for each ILR scheme with successful reductions are plotted in Figure 5. It is evident that when $\gamma$ is chosen too small, i.e., $\gamma \in [1, 8]$, not only the complexities of all schemes increase dramatically as $\gamma$ decreases, their performance degrades as well (see Figure 4). In particular, this phenomenon is more obvious for the SA-ILR methods. Indeed, their BER performance is worst than the CLLL-ILR schemes and enjoy much higher complexities. On the other hand, the constrained and unconstrained algorithms have the same $L_1$, $L_2$, iterations and FLOPs in this lower $\gamma$ range.

Afterwards, we evaluate the complexities of these schemes with larger $\gamma$ values. Evidently, according to Figure 5, the FLOPs of the SA based algorithms become close to the CLLL based ones starting from the point $\gamma = 9$ (which is also the starting point for the ideal interval of the CLLL based algorithms). In order to further study how close the performance gaps between these ILR schemes can be, we enlarge the plots of average FLOPs against $\gamma$ ranges from 9 to 20, which is illustrated in Figure 6. As we can see from it, the FLOPs of the constrained schemes and the unconstrained ones are almost the same when $\gamma \in [9, 14]$ for both CLLL-ILR and SA-ILR. Furthermore, the FLOPs of the SA-ILR and CLL-ILR algorithms are almost constants when $\gamma$ ranges from 10 to 14, and the former is just around 100 higher

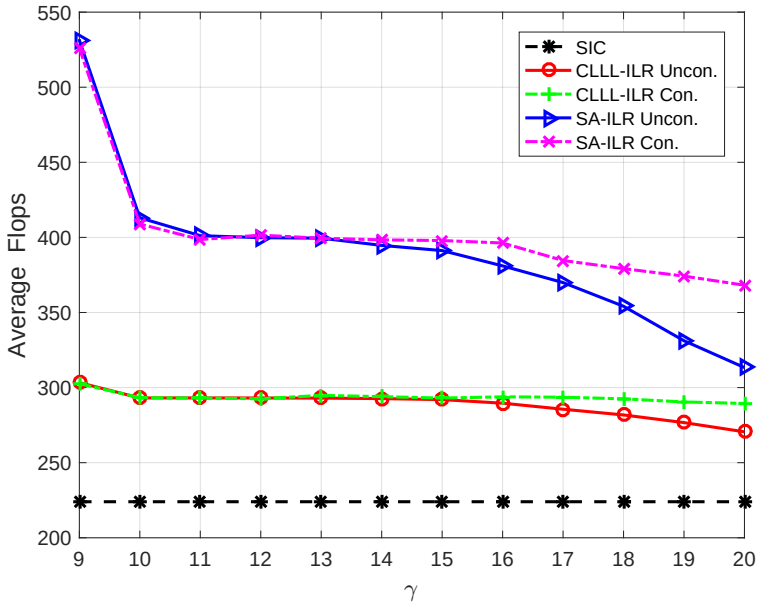


Fig. 6: The FLOPs of ILR schemes against different $\gamma$ with SNR $= 32$ dB for a 64-QAM $8 \times 8$ MIMO system under a spatial uncorrelated channel.

than the CLLL-ILR methods. On the other hand, when the RA constant $\gamma \geq 15$, the FLOPs of all schemes decrease. In addition, the decreasing speed of the constrained algorithms is slower than the corresponding unconstrained ones. This is because that the restricted schemes enjoy larger iterations of the constrained termination, i.e., the average $L_2$, as shown in Figure 5. Consequently, the BER degradation speed of the constrained methods is slower than the unconstrained ones, which can be seen from Figure 4.

*2) RA Constant in Correlated Scenario:* Now, we examine the RA constant $\gamma$ in a 16-QAM $64 \times 64$ MIMO system under the spatial correlated channel. Figure 7 illustrates the BER performance of the ILR schemes with different values of $\gamma$. Basically, by comparing it with Figure 4, we can draw the similar conclusions as in the uncorrelated scenario, except two major different observations. First, for the unconstrained ILR schemes, the feasible interval in which the SA-ILR outperforms the CLLL-ILR, i.e., $\gamma \in [4, 21]$, is much wider than that in Figure 4. Second, by introducing the constraint (in line 17 of Algorithm II) to these ILR algorithms, their BER performance degradation when $\gamma > 21$ disappears. The reason for these two differences is that 16-QAM $64 \times 64$ MIMO system is adopted here, as lower modulation order can make the system less sensitive to the variation of $\gamma$ and larger size of MIMO makes the range of effective $\gamma$ larger.

As the relationship between the complexity parameters (i.e., $L_1$, $L_2$, iterations) and the FLOPs has already been explicitly discussed in Section IV-B1, thus, we only provide the plots of the average FLOPs against $\gamma$ in Figure 8 to demonstrate how the complexity of the ILR schemes is influenced by the parameter $\gamma$ under correlated channels. It can be seen that when $\gamma$ is in the interval [4, 20], the FLOPs of constrained ILR algorithms are equal to their correspondence unconstrained algorithms while providing the same BER performance (see Figure 7). From $\gamma = 21$ on, the FLOPs of the constrained algorithms increase as a result of maintaining their BER performance. Moreover, the increase of the SA-ILR is higher than that of the CLLL-ILR. On the other hand, the FLOPs of the unconstrained schemes drop quickly as they can be terminated easier, which leads to the degradation of their BER performance.

In addition, to verify the relationship between SNR and $\gamma$, we also conducted the above simulations with other SNRs in both correlated and uncorrelated scenarios. The major observation is that, as the SNR increases, the feasible interval of $\gamma$ moves to the right along the x-axis, which results in a growth on the value of the optimal $\gamma$.

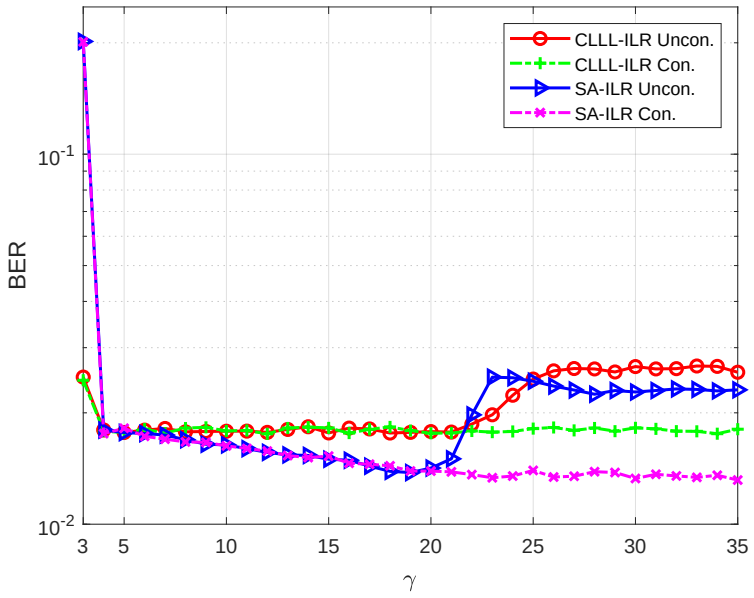


Fig. 7: The BER performance of ILR schemes against different $\gamma$ with SNR $= 35$ dB for a 16-QAM $64 \times 64$ MIMO system under a spatial correlated channel.

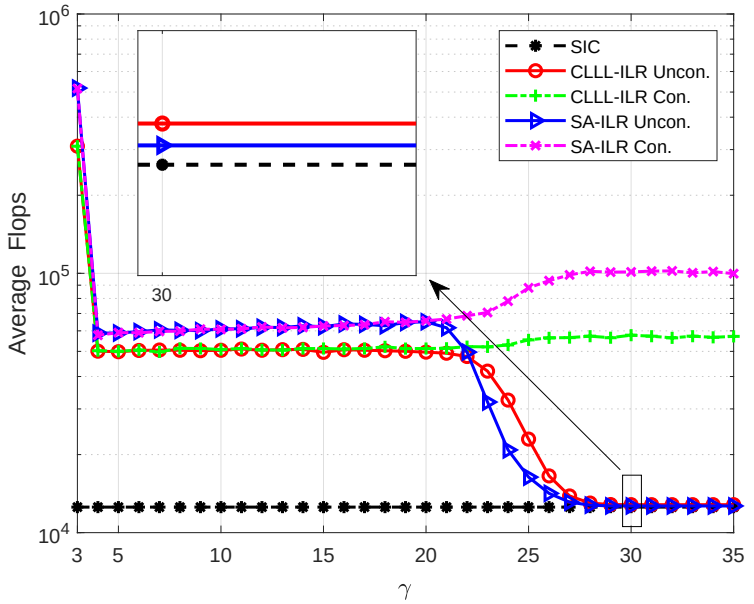


Fig. 8: The FLOPs of ILR schemes against different $\gamma$ with SNR $= 35$ dB for a 16-QAM $64 \times 64$ MIMO system under a spatial correlated channel.

### *C. Comparison between SA-ILR and CLLL-ILR*

In order to evaluate the proposed SA-ILR algorithm, the CLLL-ILR is included in the simulation as well. Similar to the SA-ILR, the CLLL-ILR is also derived from the corresponding SQR based scheme, i.e., SQR-CLLL, as given in [23]. Meanwhile, the LR aided SIC detections without ET are also utilised to examine the performance of the ILR algorithms, which includes the SQR-CLLL, SA and SQR-SA based SIC detections. Furthermore, the plain SIC detection, the ML detection and a state-of-the-art LR based method, i.e., the Lagrangian dual relaxation lattice decoding (LDR-LD) [36], are also included as performance metrics. In the following, we compare the performance of these schemes under both uncorrelated and correlated scenarios with different $\gamma$ settings, i.e., *uncorrelated scenario with fixed RA*

*constant $\gamma$, uncorrelated scenario with optimal RA constant $\gamma$* and *correlated scenario with optimal RA constant $\gamma$*. Note that the BER of all these schemes are extremely close when the SNR is low. Therefore, to observe the performance difference among these approaches, we mainly focus on the high SNR regions, i.e., [20 dB,36 dB] in the uncorrelated channel scenario and [30 dB, 45 dB] in the correlated channel scenario.

*1) Uncorrelated scenario with Fixed RA constant $\gamma$:* In conventional CLLL based ILR, the authors examined the BER performance of the proposed ILR with a fixed RA threshold parameter, which is 18.2 in their work as this value serves the most cases with a BER of $10^{-3}$ for SNR $\leq$ 33 dB (see [23]). Intuitively, as the suitable $\gamma$ that preserves a BER with $10^{-3}$ in our scenario has been obtained as well (see Figure 4), we conduct a simulation with fixed RA parameter $\gamma = 11$ at first. The BER performance against SNRs of these schemes is illustrated in Figure 9. Based on it, some conclusions can be drawn in the following.

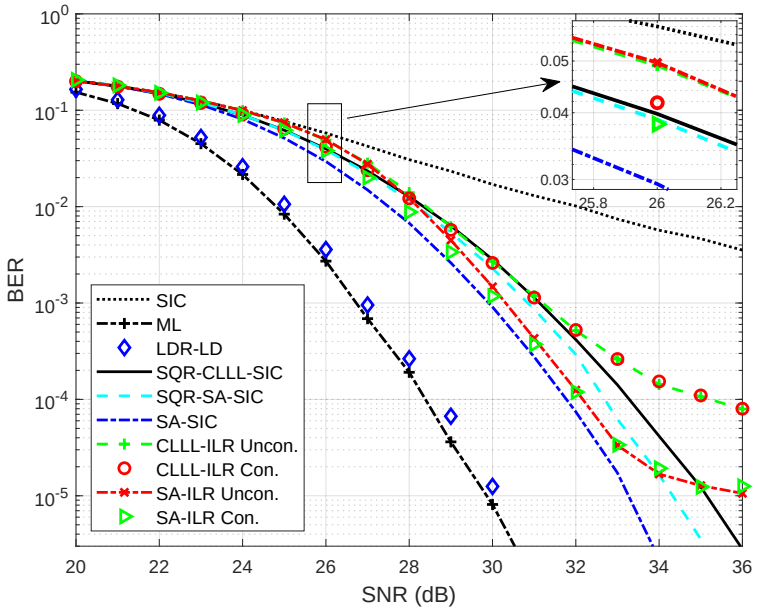


Fig. 9: The BER performance of ILR schemes against SNR with fixed $\gamma$ for a 64-QAM $8 \times 8$ MIMO system under a spatial uncorrelated channel.

Clearly, in comparison to the ML and LDR-LD methods, all ILR aided schemes have relatively lower performance, while they spend significantly less computing resource, i.e., have a quite lower complexity (which can be validated in the discussion of complexity in the following paragraphs). For a system that has fewer limits on computing resources, the ILR schemes are not preferred. On the other hand, the ILR aided schemes have a similar complexity but a higher performance than the SIC detection. Hence, it is meaningful and gainful to investigate these ILR based schemes as they are able to boost the performance of computing-resource-limited systems.

Secondly, the SA-ILR outperforms the conventional CLLL-ILR. The improvement is significant and evident in the high SNR range. When the BER is equal to $10^{-3}$, the SA based ILR is 1 dB better than the CLLL-ILR. And when the BER is required to be less than $10^{-4}$, the necessary SNR of the former is almost 4 dB less than the latter.

Thirdly, with the increasing of SNR from 20 to 31 dB, the BER performance of the CLLL-ILR and the SA-ILR are approaching to their lower bound, i.e., the BER of SQR-CLLL-SIC and SA-SIC, respectively. However, from 32 dB on, this trend stops, and the performance gaps between these ILR schemes and their corresponding lower bound are increasing on SNR. More importantly, the BER floors of these ILR approaches start to appear after 33 dB. This holds as we fixed $\gamma = 11$ in this simulation, which is too small for the ET process in the higher SNR range, thus, the termination cannot be triggered in time and leads

to estimation errors. However, this issue can be solved by choosing $\gamma$ properly, which will be discussed later on in Section IV-C2.

Fourthly, the performance of the SA-ILR is surprisingly better than the SQR-SA aided SIC detection with SNR ranges from 28 to 33 dB. This holds as though the channel matrix is not thoroughly SA reduced, during the basis update process of SA-ILR, an $\mathbf{R}$ matrix with better diagonal ordering may be achieved, which can be much closer to the $\mathbf{R}$ matrix acquired from the original SA aided SIC detection. Indeed, if $\gamma$ is chosen properly, the performance of SA-ILR should be very close to the SA-SIC detection, which is the lower bound of the BER.

Last but not least, the constrained algorithms are superior to the unconstrained ones in the BER performance. From 23 to 30 dB, they are slightly better than the unconstrained schemes. And after 31 dB, the deterioration speed of the constrained methods are relatively slower. However, they also bring the undesirable complexity increase to the system.

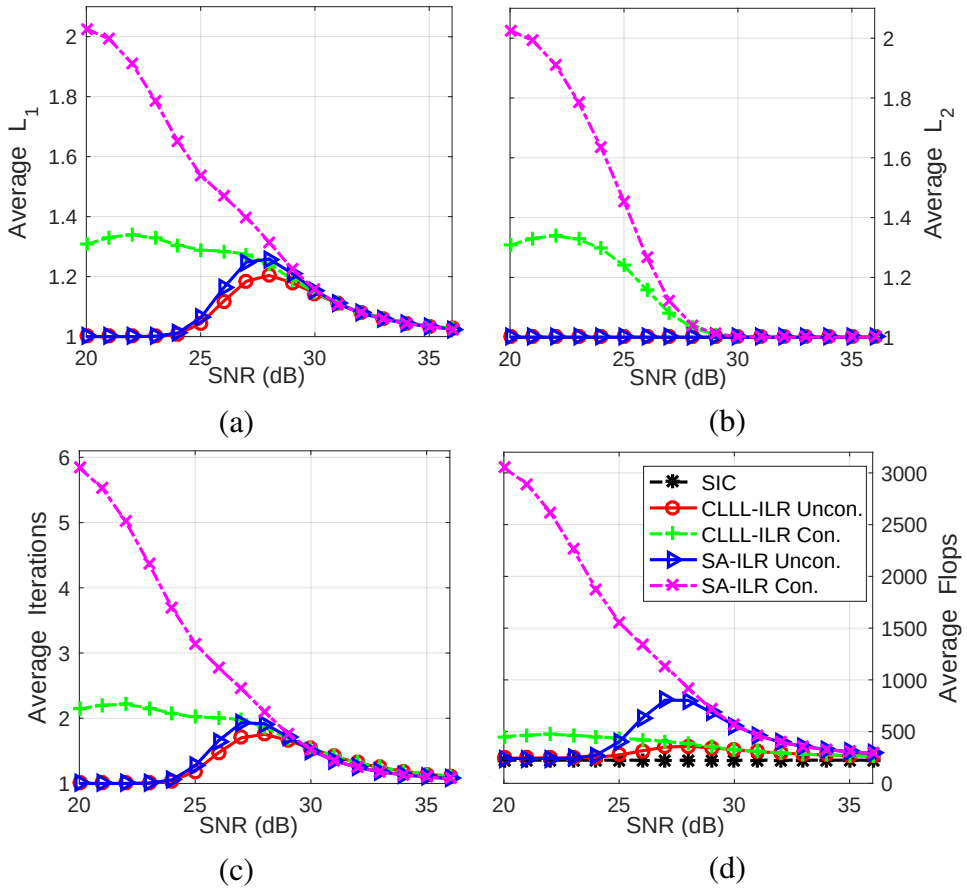


Fig. 10: The complexity parameters and FLOPs of ILR schemes against SNR with fixed $\gamma$ for a 64-QAM $8 \times 8$ MIMO system under a spatial uncorrelated channel.

Now we discuss the complexity in the following. For this system with fixed RA constant $\gamma$ under Rayleigh channel, the average $L_1$, $L_2$, iterations and FLOPs against SNR are illustrated in Figure 10.

First of all, we make a comparison between the constrained and the unconstrained algorithms. Apparently, the FLOPs of the two unconstrained algorithms are lower when SNR $\leq$ 27 dB. With the increase in SNR, they are approaching the FLOPs of the corresponding constrained algorithms. By checking the plots of average $L_2$, we can explain it easily. For the unconstrained schemes, their $L_2$ are always 1, which means the algorithm terminates easier, thus, leads to a smaller $L_1$ and less outer loop iterations. Another interesting point is that the unconstrained algorithms only begin to function when the SNR approaches 24 dB, which is the point where the LR-aided detections start to outperform the traditional SIC detection if we refer to Figure 9. Therefore, the huge amount of operations brought by the introduction of the

constraint before this point can be regarded as useless and unnecessary. Actually, before SNR $= 24$ dB, the complexity of the unconstrained algorithms are equal to the SIC detection.

After evaluating the complexities of the constrained and the unconstrained schemes, we compare the SA-ILR with the CLLL-ILR here. In general, the complexity of the former is higher than the latter, especially for the constrained scheme. When considering the unconstrained SA-ILR, there exists a relatively greater average FLOPs gap between it and the unconstrained CLLL-ILR with SNR $\in [26, 30]$ dB. However, the BER performance improvement of SA-ILR is not significant within this SNR range. Thus, we can choose a larger $\gamma$ set instead of the optimal one to reduce the complexity. From SNR $\geq 30$ dB, the BER improvement of the unconstrained SA-ILR is more obvious. It also follows that the average $L_1$, $L_2$ and iterations for both SA and CLLL based ILR schemes become the same. However, there still exists a small FLOPs gap. As discussed in Section III-D, this is because of the additional $\mathcal{O}\left(12N_t^2\right)$ FLOPs for the initialisation of the metric computation in the SA-ILR algorithms. When the average iterations turn to 1, the gap decreases and the FLOPs of all schemes approach the SIC detection. It is also worth mentioning that although the LDR-LD outperforms the proposed SA-ILR, the FLOPs of it in an $8\times8$ MIMO system with 64-QAM symbols for SNR $= 22$ dB is about $3\times10^4$, which is not in the same order of magnitude as the SA-ILR.

*2) Uncorrelated Scenario with Optimal RA constant $\gamma$:* From the analysis above, we learn that, instead of using the fixed RA parameter, the unstrained algorithms can achieve the same performance as the constrained algorithms with a set of properly selected parameters. Therefore, a rough search for parameter $\gamma$ over the integer set [4,18] for SNR ranges from 20 to 36 dB is conducted. And the corresponding optimal $\gamma$ set for both SA-ILR and CLLL-ILR is $[9, 9, 9, 9, 9, 9, 9, 9, 10, 10, 10, 11, 12, 12, 12, 12, 12]$. They have the same optimal $\gamma$ set because, on the one hand, this is the optimal set based on the rough search. On the other hand, we also have shown that the optimal $\gamma$ of SA-ILR is also the optimal one of CLLL-ILR in the previous simulation in Section IV-B.

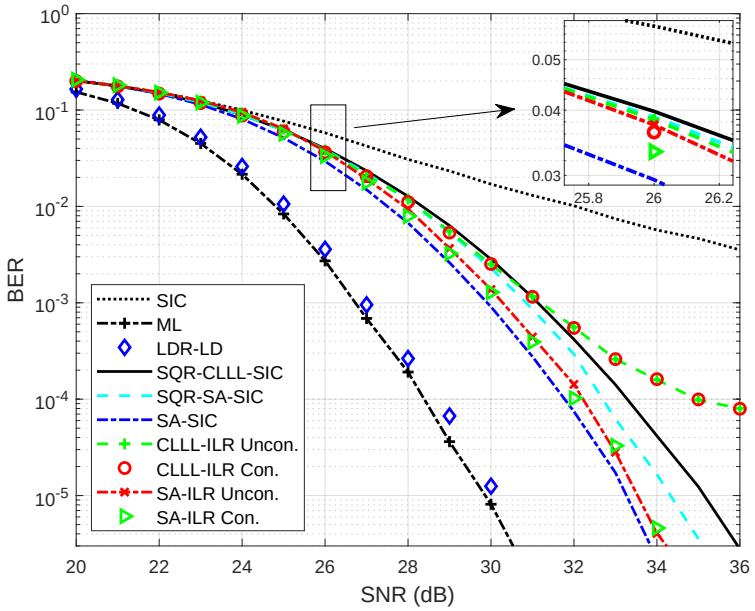


Fig. 11: The BER performance of ILR schemes against SNR for 64-QAM a $8\times8$ MIMO under a spatial uncorrelated channel with optimal $\gamma$.

We first investigate the BER performance of these ILR schemes, which is shown in Figure 11. Two major observations can be achieved by comparing it with Figure 9. First, the performance of all algorithms is improved in the lower SNR range from 23 to 27 dB, especially for the unconstrained cases. Second, for the higher SNR part, both SA based ILR algorithms benefit from the new $\gamma$ set. Their performance is close to the conventional SA based detection, and the unconstrained one matches the constrained algorithm

perfectly. More importantly, the error floors presented in Figure 9 for SA-ILR schemes in the higher SNR range vanished, which validates that selecting $\gamma$ appropriately is an effective solution to the error floors. On the contrary, the performance of the CLLL based ILR algorithms in this higher SNR range is not improved significantly by choosing $\gamma$ optimally.

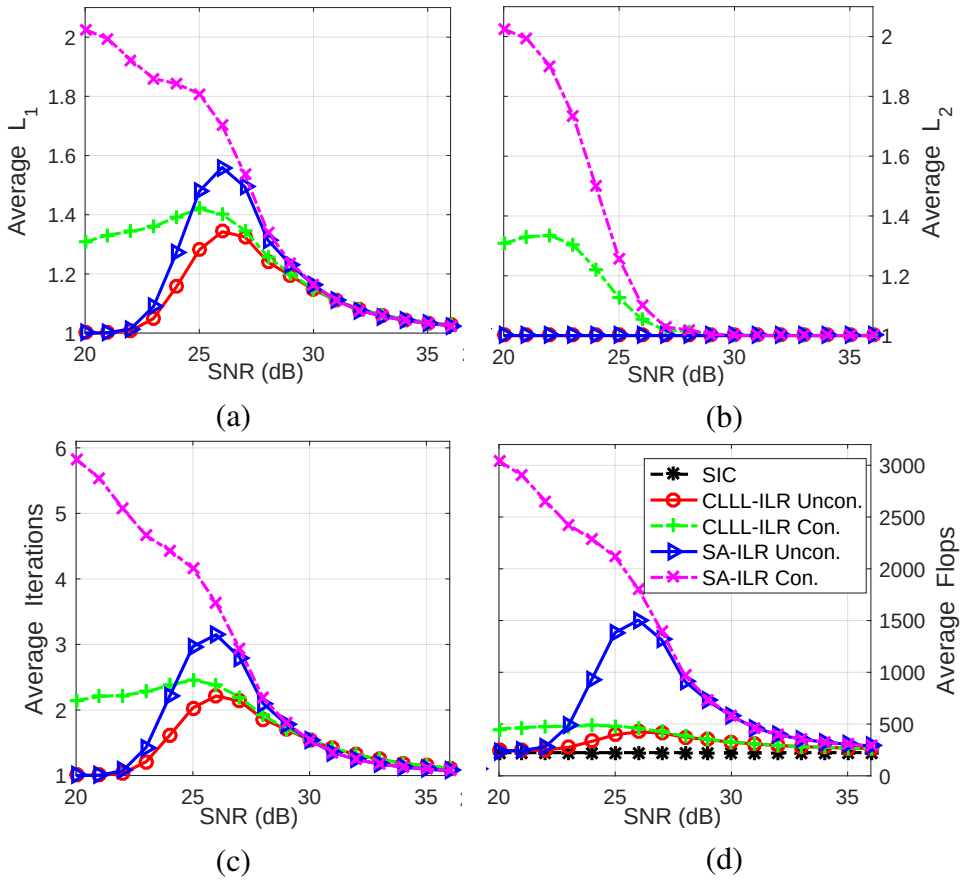


Fig. 12: The complexity parameters and FLOPs of ILR schemes against SNR for a 64-QAM $8 \times 8$ MIMO system under a spatial uncorrelated channel with optimal $\gamma$.

Afterwards, we analyse how the complexities of the SA-ILR and CLLL-ILR algorithms are influenced by introducing the optimal $\gamma$ set into them. Similar to the case with fixed $\gamma$ under Rayleigh channel, the average number of $L_1$, $L_2$, outer iterations and FLOPs against SNRs are also given in Figure 12. Definitely, by comparing with the plots in Figure 10, the overall complexity of all ILR schemes is increased in this case. For the lower SNR range, most of the complexity increase is between 23 to 27 dB, which is just the interval that the BER of all ILR schemes is improved noticeably as analysed in the previous paragraph. In addition, also in this SNR interval, we can observe that the complexity growth brought by the optimal $\gamma$ for the SA-ILR is higher than for the CLLL-ILR. Similarly, this complexity growth trend can be applied to the constrained and unconstrained algorithms either, in which the constrained one experience more complexity increase when compared to the corresponding unconstrained scheme. Starting from SNR = 28 dB, the growth in the FLOPs of all ILR algorithms is negligible. However, the BER performance improvement for the SA-ILR methods is significant by referring to Figure 9 and Figure 11. It should be mentioned that the average FLOPs of SA-ILR algorithms is still greater than that of the CLLL-SA schemes in the higher SNR range, which is different from the results that will be discussed in the correlated scenario.

To further verify the performance-complexity tradeoff of the ILR schemes, we utilise a utility function to ease the analysis, which is defined as $\Lambda = P_e N_F$, where $P_e$ and $N_F$ represent the value of BER and the number of FLOPs, respectively. Apparently, under the same conditions, the smaller the value of $\Lambda$, the better the algorithm performs. Figure 13 illustrates $\Lambda$ against different SNRs for ILR schemes and the SIC

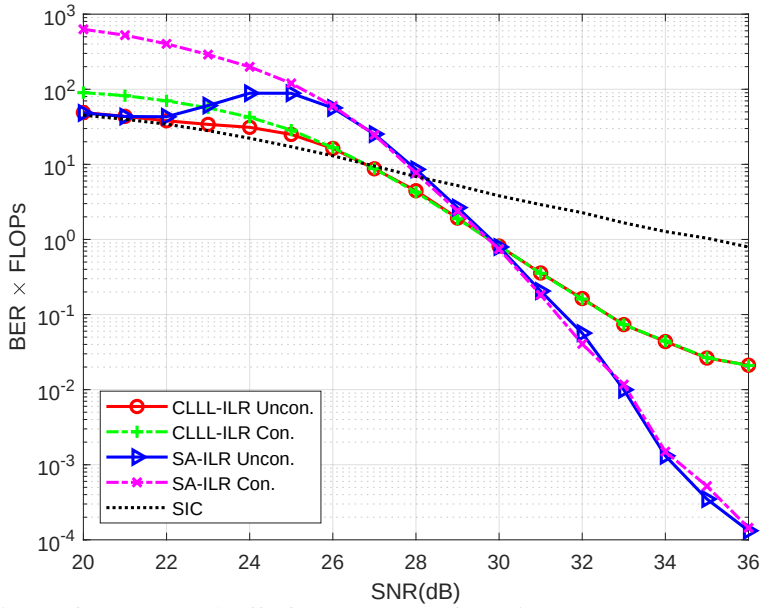


Fig. 13: The complexity-performance tradeoff of ILR schemes for a 64-QAM $8 \times 8$ MIMO system under a spatial uncorrelated channel with optimal $\gamma$.

detection. It can be observed that from 20 dB to 26 dB, the SIC detector is superior to all ILR schemes. With the increase of SNR, CLLL-ILR schemes start to outperform SIC and SA-ILR detectors. However, when the SNR is larger than 30 dB, SA-ILR algorithms surpass CLLL-ILR schemes as well as the SIC detector. Moreover, the advantage of SA-ILR schemes becomes more significant as the SNR increases. On the other hand, when comparing the constrained ILR schemes with the corresponding unconstrained approaches, the latter is always better or at least equal to the former.

*3) Correlated Scenario with Optimal RA constant $\gamma$:* In this part, we evaluate the performance of the proposed SA-ILR schemes under the spatial correlated channel. The optimal $\gamma$ set for both SA-ILR and CLLL-ILR approaches in this scenario with SNR from 30 dB to 45 dB is [10, 12, 14, ..., 39]. Similar to Section IV-C2, we first examine the BER performance of SA-ILR schemes by comparing with CLLL-ILR and other detection methods, as shown in Figure 14. In general, the behaviour of these schemes are quite similar to that in the uncorrelated scenario (see Figure 11). The most significant difference is that SA-ILR based schemes surprisingly outperform the SA-SIC detector, which is supposed to be the lower bound of SA-ILR algorithms. This holds as when introducing the spatial correlation into the channel matrix, the positive effect of fully SA reduction is diminished. However, during the intermediate steps of SA, a non-fully reduced channel matrix may mitigate the influence brought by the spatial correlation, thus facilities the SIC to produce better detection results.

Now, we compare the complexity of SA and CLLL based ILR algorithms in the correlated scenario. As the relationship between the complexity parameters and the FLOPs has already been discussed in Section IV-C2, and this does not change, thus we only provide the simulation results of FLOPs against SNR here, as given in Figure 15. It can be seen that the plots in this figure actually corresponding to the plots with SNR ranges from 27 dB to 36 dB in Figure 12d. Note that a logarithmic scale is used for the y-axis in Figure 15 to provide better illustration. By comparing these two figures, most conclusions drawn in the uncorrelated scenario of Section IV-C2 apply to here either. The greatest difference is that, in this scenario, starting from SNR $= 39$ dB, the average FLOPs of the SA-ILR becomes lower than that of the CLLL-ILR. This is significant, especially considering that their BER is also evidently lower than CLLL-ILR schemes' BER in this SNR range, which makes the SA-ILR superior to CLLL-ILR in both complexity and performance.

Finally, the tradeoff between the complexity and the performance of both SA and CLLL based ILR

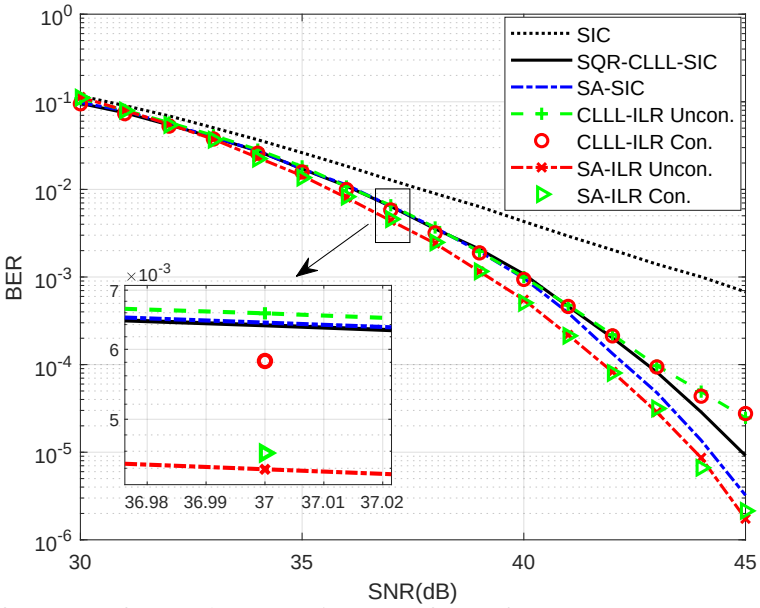


Fig. 14: The BER performance of ILR schemes against SNR for a 16-QAM $64 \times 64$ MIMO system under a spatial correlated channel with optimal $\gamma$.

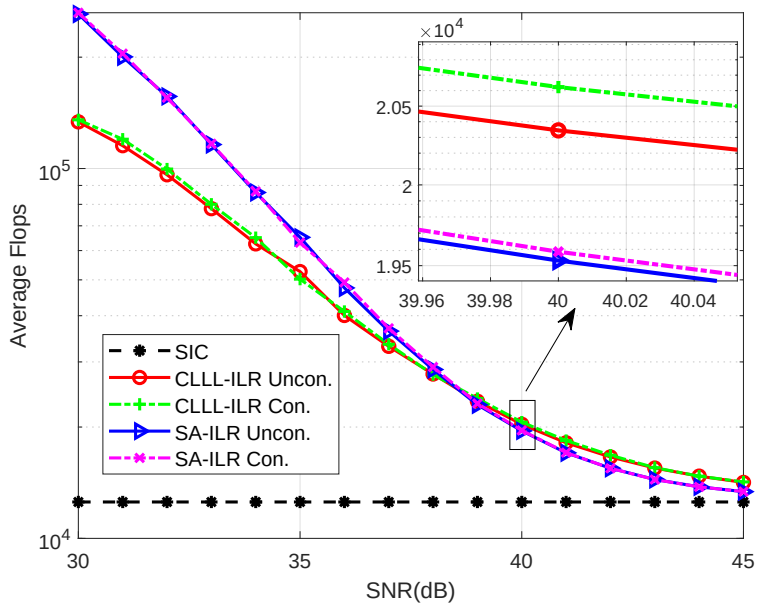


Fig. 15: The FLOPs of of ILR schemes against SNR for a 16-QAM $64 \times 64$ MIMO system under a spatial correlated channel with optimal $\gamma$.

algorithms is analysed by utilising the same utility function. The simulation results are provided in Figure 16. It can be observed that, unlike in the uncorrelated scenario with optimal $\gamma$, CLLL-ILR schemes cannot outperform both SIC and SA-ILR methods at the same time throughout the whole SNR range. In other words, when considering both complexity and BER performance in the system design, the SIC detector should be employed when SNR $<$ 37 dB while SA-ILR schemes must be utilised when SNR $\geq$ 37 dB.

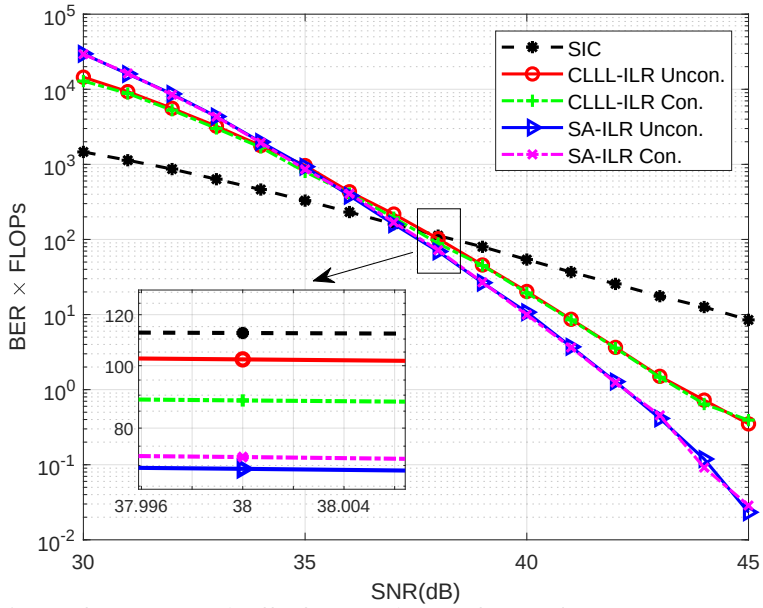


Fig. 16: The complexity-performance tradeoff of ILR schemes for a 16-QAM $64 \times 64$ MIMO system under a spatial correlated channel with optimal $\gamma$.

## V. Conclusions

In this paper, two novel algorithms are introduced in order to apply SA to ILR. First, the proposed SQR-SA algorithm offers a new SA reduction solution by updating the matrices that are obtained from the QR decomposition. Second, the proposed SA aided ILR algorithm allows performing the SA reduction together with the SIC detection and terminating the process at the ideal time. They are explicitly explained using detailed pseudo-codes. Afterwards, the effectiveness of the SQR-SA algorithm is validated by simulation results first as it plays the key role in the SA based ILR scheme. To evaluate the performance of the SA-ILR, conventional CLLL based ILR is utilised for comparison. Two variants, the constrained and unconstrained cases for both SA and CLLL based methods are studied. According to the simulations, the proposed SA-ILR outperforms the CLLL-ILR entirely concerning the BER performance. More importantly, in high SNR regions, the complexity of the SA-ILR is lower than that of the CLLL-ILR in the correlated channel, while only slightly higher than the complexity of the CLLL-ILR in the uncorrelated channel. In low SNR ranges, the cost on the complexity is acceptable if the unconstrained SA-ILR is utilised with an appropriately chosen RA parameter set.

## References

[1] Alsharif Mohammed H., Nordin Rosdiadee, Abdullah Nor Fadzilah, Kelechi Anabi Hilary. How to make key 5G wireless technologies environmental friendly: A review. *Trans Emerg Telecommun Technol.* 2018;29(1):e3254.

[2] Arash Masoud, Yazdian Ehsan, Fazel Mohammad Sadegh, Brante Glauber, Imran Muhammad Ali. Employing antenna selection to improve energy efficiency in massive MIMO systems. *Trans Emerg Telecommun Technol.* 2017;28(12):e3212.

[3] Marinello Filho José Carlos, Panazio Cristiano Magalhães, Abrão Taufik. Joint uplink and downlink optimization of pilot assignment for massive MIMO with power control. *Trans Emerg Telecommun Technol.* 2017;28(12):e3250.

[4] Abediseid Walid. On the average complexity of sphere decoding in lattice space–time coded multiple-input multiple-output channel. *Trans Emerg Telecommun Technol.* 2015;26(3):355-366.

[5] Shin Sang-Sik, Choi Hongsoo, Jang Jae-Eun, Choi Ji-Woong. A low-complexity iterative MIMO detection and decoding scheme using dimension reduction. *Trans Emerg Telecommun Technol.* 2016;27(1):136-145.

[6] Fukuda Rafael Masashi, Guerra David William Marques, Kobayashi Ricardo Tadashi, Abrão Taufik. DE/PSO-aided hybrid linear detectors for MIMO-OFDM systems under correlated arrays. *Trans Emerg Telecommun Technol.* 2018;29(12):e3495.

[7] Pereira Jr Alexandre A., Sampaio-Neto Raimundo. Low-complexity soft-output MIMO uplink detection for large systems iterative detection and decoding. *Trans Emerg Telecommun Technol.* 2018;29(2):e3251.

[8] Wubben D., Seethaler D., Jalden J., Matz G. Lattice reduction. *IEEE Signal Process Mag.* 2011;28(3):70-91.

[9] Negrão João Lucas, Abrão Taufik. Efficient detection in uniform linear and planar arrays MIMO systems under spatial correlated channels. *Int J Commun Syst.* 2018;31(11):e3697.

[10] Kobayashi Ricardo Tadashi, Ciriaco Fernando, Abrão Taufik. Efficient near-optimum detectors for large MIMO systems under correlated channels. *Wireless Pers Commun.* 2015;83(2):1287–1311.

[11] Valente Raul Ambrozio, Marinello José Carlos, Abrão Taufik. LR-aided MIMO detectors under correlated and imperfectly estimated channels. *Wireless Pers Commun.* 2014;77(1):173–196.

[12] Ma X., Zhang W. Performance analysis for MIMO systems with lattice-reduction aided linear equalization. *IEEE Trans Commun.* 2008;56(2):309-318.

[13] Wubben D., Bohnke R., Kuhn V., Kammeyer K. D. Near-maximum-likelihood detection of MIMO systems using MMSE-based lattice-reduction. Paper presented at: 2004 IEEE International Conference on Communications (ICC); June 2004; Paris, France.

[14] Taherzadeh M., Mobasher A., Khandani A. K. LLL Reduction achieves the receive diversity in MIMO decoding. *IEEE Trans Inf Theory.* 2007;53(12):4801-4805.

[15] Barbero L. G., Ratnarajah T., Cowan C. A comparison of complex lattice reduction algorithms for MIMO detection. Paper presented at: 2008 IEEE International Conference on Acoustics, Speech and Signal Processing (ICASSP); April 2008; Las Vegas, NV, USA.

[16] Wubben D., Bohnke R., Rinas J., Kuhn V., Kammeyer K. D. Efficient algorithm for decoding layered space-time codes. *Electronics Lett.* 2001;37(22):1348-1350.

[17] Ling C., Howgrave-Graham N. Effective LLL reduction for lattice decoding. Paper presented at: 2007 IEEE International Symposium on Information Theory (ISIT); June 2007; Nice, France.

[18] Gan Y. H., Ling C., Mow W. H. Complex Lattice Reduction Algorithm for Low-Complexity Full-Diversity MIMO Detection. *IEEE Trans Signal Process.* 2009;57(7):2701-2710.

[19] Vetter H., Ponnampalam V., Sandell M., Hoeher P. A. Fixed complexity LLL algorithm. *IEEE Trans Signal Process.* 2009;57(4):1634-1637.

[20] Ling C., Mow W. H., Howgrave-Graham N. Reduced and fixed-complexity variants of the LLL algorithm for communications. *IEEE Trans Commun.* 2013;61(3):1040-1050.

[21] Wen Q., Zhou Q., Ma X. An enhanced fixed-complexity LLL algorithm for MIMO detection. Paper presented at: 2014 IEEE Global Communications Conference (GLOBECOM); December 2014; Austin, TX USA.

[22] Wang W., Hu M., Li Y., Zhang H., Li Z. Computationally efficient fixed complexity LLL algorithm for lattice-reduction-aided multiple-input–multiple-output precoding. *IET Commun.* 2016;10(17):2328-2335.

[23] Gestner B., Ma X., Anderson D. V. Incremental lattice reduction: motivation, theory, and practical implementation. *IEEE Trans Wireless Commun.* 2012;11(1):188-198.

[24] Wang F., Xiong Y., Yang X. Reliability assessment for MIMO detection and its application. *Int. J of Electron and Commun.* 2009;63(8):678 - 684.

[25] Kim Hyunsub, Lee Hyukyeon, Koo Jihye, Kim Jaeseok. Low-complexity lattice reduction algorithm for MIMO detectors with tree searching. *Eur J Wireless Commun Netw.* 2017;2017(1):17.

[26] Seysen M. Simultaneous reduction of a lattice basis and its reciprocal basis. *Combinatorica.* 1993;13(3):363–376.

[27] Bruderer L., Senning C., Burg A. Low-complexity Seysen's algorithm based lattice reduction-aided MIMO detection for hardware implementations. Paper presented at: 2010 Conference Record of the Forty Fourth Asilomar Conference on Signals, Systems and Computers; November 2010; Pacific Grove, CA, USA.

[28] Sheikh F., Balatsoukas-Stimming A., Chen C. H. High-throughput lattice reduction for large-scale MIMO systems based on Seysen's algorithm. Paper presented at: 2016 IEEE International Conference on Communications (ICC); May 2016; Kuala Lumpur, Malaysia.

[29] Seethaler D., Matz G., Hlawatsch F. Low-Complexity MIMO Data Detection using Seysen's Lattice Reduction Algorithm. Paper presented at: 2007 IEEE International Conference on Acoustics, Speech and Signal Processing (ICASSP); April 2007; Honolulu, HI, USA.

[30] Niu J., Lu I. A comparison of two lattice-reduction-based receivers for MIMO systems. Paper presented at: 2008 IEEE Sarnoff Symposium; April 2008; Princeton, NJ, USA.

[31] Hassibi B.. An efficient square-root algorithm for BLAST. Paper presented at: 2000 IEEE International Conference on Acoustics, Speech, and Signal Processing (ICASSP); June 2000; Istanbul, Turkey.

[32] Clarkson I. Vaughan L. Approximation of Linear Forms by Lattice Points with Application to Signal Processing. *PhD thesis*: The Australian National University; 1997.

[33] Gestner B., Zhang W., Ma X., Anderson D. V. Lattice Reduction for MIMO Detection: From Theoretical Analysis to Hardware Realization. *IEEE Trans Circuits Syst I, Reg Papers.* 2011;58(4):813-826.

[34] Zhang W., Ma X., Swami A. Designing low-complexity detectors based on Seysen's algorithm. *IEEE Trans Wireless Commun.* 2010;9(10):3301-3311.

[35] Kermoal J. P., Schumacher L., Pedersen K. I., Mogensen P. E., Frederiksen F. A stochastic MIMO radio channel model with experimental validation. *IEEE J Sel Areas Commun.* 2002;20(6):1211-1226.

[36] Pan J., Ma W., Jaldén J. MIMO detection by Lagrangian dual maximum-likelihood relaxation: reinterpreting regularized lattice decoding. *IEEE Trans Signal Process.* 2014;62(2):511-524.